

UNCLASSIFIED

AD NUMBER
AD879684
NEW LIMITATION CHANGE
TO Approved for public release, distribution unlimited
FROM Distribution authorized to U.S. Gov't. agencies and their contractors; Critical Technology; OCT 1970. Other requests shall be referred to Air Force Avionics Laboratory, Attn: AFAL/WRE, Wright-Patterson AFB, OH 45433.
AUTHORITY
afal ltr, 18 jun 1974

THIS PAGE IS UNCLASSIFIED

AFAL-TR-70-137

20

AD879684

TRIBOELECTRIC CHARGING OF AIRCRAFT DIELECTRIC SURFACES IN THE MICROWAVE FREQUENCY REGION (1-4 GHz)

LARRY E. CUMMINGS

TECHNICAL REPORT AFAL-TR-70-137

OCTOBER 1970



This document is subject to special export controls and each transmittal to foreign governments or foreign nationals may be made only with prior approval of the Air Force Avionics Laboratory (AFAL/WRE), Wright-Patterson Air Force Base, Ohio 45433.

AIR FORCE FLIGHT DYNAMICS LABORATORY
AIR FORCE SYSTEMS COMMAND
WRIGHT-PATTERSON AIR FORCE BASE, OHIO

AFC
RECEIVED
FEB 8 1971
C

41

NOTICE

When Government drawings, specifications, or other data are used for any purpose other than in connection with a definitely related Government procurement operation, the United States Government thereby incurs no responsibility nor any obligation whatsoever; and the fact that the government may have formulated, furnished, or in any way supplied the said drawings, specifications, or other data, is not to be regarded by implication or otherwise as in any manner licensing the holder or any other person or corporation, or conveying any rights or permission to manufacture, use, or sell any patented invention that may in any way be related thereto.

ACCESSION for	
CPSTI	WHITE SECTION <input type="checkbox"/>
DDC	BLUE SECTION <input checked="" type="checkbox"/>
UNANNOUNCED	<input type="checkbox"/>
JUSTIFICATION	
BY	
DISTRIBUTION/AVAILABILITY CODES	
DIST.	AVAIL. and/or SPECIAL
2	

Copies of this report should not be returned unless return is required by security considerations, contractual obligations, or notice on a specific document.

AFAL-TR-70-137

**TRIBOELECTRIC CHARGING OF AIRCRAFT DIELECTRIC
SURFACES IN THE
MICROWAVE FREQUENCY REGION (1-4 GHz)**

LARRY E. CUMMINGS

This document is subject to special export controls and each transmittal to foreign governments or foreign nationals may be made only with prior approval of the Air Force Avionics Laboratory (AFAL/WRE), Wright-Patterson Air Force Base, Ohio 45433.

The distribution of this report is limited because it contains conclusions and recommendations for future research and development plans in relation to military weapons systems.

FOREWORD

This report was prepared by the Air Force Avionics Laboratory, Wright-Patterson Air Force Base, Ohio. The information presented in this report is the result of in-house work performed during the period from May 1969 to March 1970 at the Electromagnetic Compatibility Research Facility of the Experimental Evaluation Group, Electromagnetic Environment Branch, AFAL/WRE. The work was accomplished under Task 435706, "Natural RF Interference and Electrical Hazards for Air Force Aerospace Vehicles," Project 4357, "Electromagnetic Compatibility Techniques." The project engineer was Mr. H. M. Bartman. Mr. Larry E. Cummings was the principal investigator. This report was submitted by the author April 1970.

The author expresses his appreciation to Messrs. Herbert M. Bartman and Claude R. Austin for their helpful suggestions and constructive criticism during the actual work effort and preparation of this manuscript.

This technical report has been reviewed and is approved.


RAYMOND J. MORDLUND
Chief Scientist
Air Force Avionics Laboratory

ABSTRACT

Triboelectric charging can cause serious problems to modern aircraft. This work effort attempts to determine the RF spectral content of streamers produced on various dielectric materials that are being used or could be used on future high performance aircraft. These values are found to be in good agreement with the theoretically derived spectrum.

This investigation covered the frequency range of 1.0 GHz to 4.0 GHz. Such a range is convenient in that it starts where other researchers have stopped and gives a good indication of expected signal levels at higher frequencies. A more detailed study could also be conducted due to the small frequency span.

The first part of this report discusses the experimental setup and the rationale for the procedures used. Based on the experimental values obtained, definite recommendations are made for the reduction of precipitation static interference. The values obtained show a close correlation with flight test data.

TABLE OF CONTENTS

SECTION	PAGE
I INTRODUCTION	1
1. Purpose	1
2. Background	1
II TRIBOELECTRIC CHARGING OF AIRCRAFT SURFACES	4
III THE TESTING ENVIRONMENT	5
IV TEST EQUIPMENT	11
V SYSTEM CALIBRATION	13
VI TEST SAMPLES	19
VII SAMPLE POSITIONING	24
VIII RESULTS	25
IX TEST DIFFICULTIES TO BE EXPECTED	42
X CONCLUSIONS AND RECOMMENDATIONS	45
1. Conclusions	45
2. Recommendations	46
APPENDIX I DISCUSSION OF SPARKING MECHANISM	49
APPENDIX II NATURAL VERSUS ARTIFICIAL ENVIRONMENT	53
APPENDIX III DERIVATION OF THEORETICAL SPECTRUM	57
REFERENCES	60

ILLUSTRATIONS

FIGURE	PAGE
1. Side View of Testing Chamber	6
2. Top View of Chamber	6
3. Breakdown Voltage Correction Factor Versus Relative Humidity	10
4. Range of Computed Stream Velocities	14
5. Typical Memoscope Trace	15
6. Impulse Response	17
7. Test Samples	21
8. Slotted Metallic RF Window Samples	22
9. Computed Generated Signal Strengths (Mounting Method A)	26
10. Average Received Signal Strength (Mounting Method B)	27
11. Computed Generated Signal Strengths (Mounting Method B)	29
12. Generated Signal Strength Envelopes	31
13. Noise Normalized to Aircraft Sample	32
14. Teflon Pulses	33
15. Plexiglas Pulses	33
16. Polyester-Coated SMRFB(B) Pulses on Polyester Layer	34
17. Polyester-Coated SMRFB(B) Pulses on Metal Layer	34
18. Epoxy Pulses	35
19. Aircraft Sample Pulse Train at 50 microseconds/cm	36
20. Aircraft Sample Pulse Train at 20 microseconds/cm	36

ILLUSTRATIONS (CONT)

FIGURE	PAGE
21. Illustration of Multiple Pulse Theory	37
22. Teflon Pulse Path Decay	38
23. Theoretical Spectrum of Fast Rise-Time Pulses	39
24. Quartz Static Field	41
25. Epoxy Static Field	41
26. Particle Density Profile	54

TABLES

TABLE		PAGE
I	HP 425A Input Resistance	12
II	Particle Velocity Standard Deviations	13
III	Observed Rise-Time Errors	18
IV	Receiver Pulse Response	18
V	Physical Constants	23
VI	Line Equations for Figure 9	25
VII	Line Equations for Figure 11	28
VIII	Comparative Readings	30
IX	Pulse Parameters (Across 50 Ohms)	35
X	DC Currents of Samples	40
XI	Variation of a With X/p	52
XII	Average Free Electrical Charge on Individual Droplets	55
XIII	Breakdown Voltage Versus Altitude	56

SECTION I
INTRODUCTION

1. PURPOSE

The purpose of this report is to alert aircraft designers and associated engineers in the radio frequency (RF) noise generating properties of selected dielectric materials in current or projected use.

Areas examined include wide band noise spectra and pulse rise times and structures; also particle size, particle velocity, particle concentration, and comparison of testing environment to natural environment. In this study, other areas were also examined and are discussed at the appropriate time.

A check of available laboratory or flight test data revealed the absence of measured noise levels above 1 GHz. Selected samples were tested to a higher frequency and the implications are discussed. The laboratory measured data is also compared to theoretically derived noise spectra.

The intended end result is to be a guide or handbook which will enable the designer to estimate the expected precipitation static noise produced under a given set of circumstances. The tabulated values are not worst case conditions but can be expected to vary widely (most probably on the high side) due to the number of variables and the extremely random nature of the process itself.

2. BACKGROUND

Particles in the flight path of an aircraft deposit a charge on a dielectric surface when they collide with it. The high resistivity of this surface will cause a high difference of potential to exist between the dielectric and the surrounding metal structure. If the resistivity is high enough, the conduction current may be smaller than the charging current. Now the electric field may reach the breakdown value for air. Arcs or streamers occur from the dielectric to the metal structure. This discharge is in effect a small lightning bolt and is an energetic, broadband RF radiator.

Precipitation static problems occur on aircraft and missiles. LORAN systems are particularly vulnerable because of their low operating frequency. Problems have been encountered on some of the big super jets and their communication systems. Instrument landing systems (ILS) have also been subject to precipitation static interference. If the effects of this phenomenon were responsible for an accident, the fact would probably be very hard to prove. In such cases the verdict may be pilot error. Under these circumstances factual fault finding may prove to be very difficult and may have to rely on a pattern of accident occurrences. This technique is highly undesirable.

An operational missile has experienced interference (thought to be precipitation static) causing its computer to dump its entire guidance memory resulting in destruction of the missile (initiated by the ground safety officer) and on-board experiments, if any. Such a circumstance could impose grave restrictions on a nation's retaliatory capacity and would be a valuable intelligence morsel for the adversary.

The trend in aircraft construction is the elimination of heavy metal for lightweight fiber-metal matrix composites or dielectric plastic or epoxy surfaces where applicable. One aircraft manufacturer has published a technical paper with a picture of an aircraft showing the in-roads made by composites. It depicts a vehicle 6 years in the future with metal used for the wing tip tanks, engine exhaust, and portions of the vertical stabilizer. Today some of our larger operational aircraft possess considerable areas of dielectric and/or fiber-metal matrix composites other than the radome. Therefore, since precipitation static is a problem today, the aircraft of the future will pose a more serious problem under the same environmental conditions unless preventive steps are taken.

One would expect precipitation static to be worse as the velocity is increased. This is true to a certain extent. Recent laboratory studies (Reference 1) indicate that triboelectric charging by ice crystals goes to zero at speeds greater than 3150 ft/sec because of crystal melting. The same study indicated that at speeds in

excess of 4000 ft/sec frictional charging by dust particles reaches zero. Apparently the dust particles form craters on impact and become buried in the material. Heat buildup will cause the dielectric resistivity to decrease. Alumina, for example, experiences a decrease in resistivity by a factor of 1000 from 500°F to 1400°F (Mach 2.5 to 4.5). As velocity increases, the area of impact becomes smaller due to shock and airflow effects.

All aircraft must eventually take off, land, and spend a portion of their flight profile in realms where precipitation static is a potential source of interference. Three courses are available and may be used separately or simultaneously; reduce or eliminate the source of the interference, reduce the damaging effects of the interference after it has been produced, and modify the coupling paths. The results of this report should enable the designer to reduce the magnitude of the interference at the source.

SECTION II

TRIBOELECTRIC CHARGING OF AIRCRAFT SURFACES

Triboelectric charging is simply static electrification by friction. The charging particles (i.e. crystals, sand, water vapor, dust, and debris from nuclear clouds) charge a dielectric surface (aircraft radomes, or nonmetallic panels) to a high potential. This potential occurs in localized areas of the surface due to the very nature of a dielectric, extremely high surface resistance. A small portion may be charged to a high enough potential to cause a small protrusion on the surface to corona, thereby producing RF noise. Furthermore, adjacent areas will become charged at different potentials. These potentials may be large enough to cause an arc (a streamer) between the two areas in an effort to equalize the charge. Naturally, this arc is a source of RF noise. Some points near the metallic portions of the airframe may arc or spark to the lower potential airframe producing more RF noise.

RF noise is the common denominator to this interference problem; i.e., its spectrum content, amplitude, dependence on the dielectric surface, and its prediction and elimination of its effect on the airborne electronics. The problem encompasses a large frequency span up to the GHz region. As on-board receiving systems become more and more sensitive, triboelectric charging of aircraft surfaces will become more important particularly when considered in relation to its deleterious effects on airborne sensitive receiving systems located behind the dielectric material or on other on-board systems having good coupling between the noise source and the appropriate antenna.

Designers of future aircraft appear to contemplate the widespread usage of dielectric materials for various fuselage parts in order to save weight and costs. Such a move may seem to be reasonable. Now suppose the RF noise level due to streamering on these surfaces is more serious than was anticipated. Several choices are available: scrap the aircraft, redesign the RF systems, or find a fix. These decisions have one thing in common: an extremely high price tag to remedy the effects of faulty thinking or inadequate research.

Some special-purpose aircraft may possess 100 or more antennas whose spatial locations are primarily determined by operational requirements. These requirements may also necessitate the need for very sensitive and/or broad-band RF receiving systems. Trouble may arise if the operations people place the antennas in such a position to cause their dielectric protective radomes or caps to be subject to triboelectric charging.

SECTION III

THE TESTING ENVIRONMENT

In any type of experimental investigation of a natural phenomenon, the first order of business is the reproduction of naturally occurring events.

A large chamber 6 ft x 4 ft x 4 ft was constructed of 1/2 inch Plexiglas. See Figures 1 and 2. Positioning rails were installed to allow the operator to position the sample with respect to distance and orientation from the charging source. The bottom of the chamber is a large funnel of heavy gauge aluminum. This arrangement allows the charging particles to fall into a receptacle for collection during operation. A high pressure spray gun serves as the accelerator for the charging particles. The gun is positioned inside the chamber and is connected to the outside by a rubberized nylon boot. The operator can manipulate the air gun and not disturb the charging environment. The interior is completely waterproof and relatively air tight when the funnel output is closed. This type of construction permits the using of water vapor, ice crystals, dust, or other charging media such as flour and potentially dangerous substances such as lycopodium powder.

Isolating the environment is very important. This chamber has been evacuated to 400 ft above ambient altitude. This figure is not at all impressive but two important facts must be borne in mind. The evacuation was stopped because of

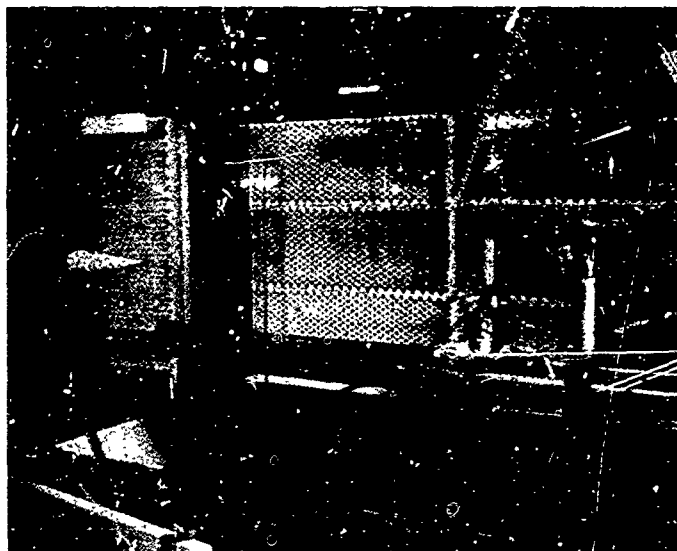


Figure 1. Side View of Testing Chamber



Figure 2. Top View of Chamber

the buckling of the aluminum side panels of the funnel and air leakage caused by the stitching in the boot around the air gun. Minor modifications should allow the pressure to be reduced to the point where flexing of the Plexiglas is the limiting factor.

Additional variables may be added to the experimental program by utilizing some of the chamber's properties. Ultraviolet lighting may be added to simulate the type of radiation encountered at high altitudes. Field strengths of 6000 volts/meter and higher are encountered in the vicinity of thunderstorms (Reference 2). These potentials can easily be incorporated into the program. A near miss by a bolt of lightning will also deposit a considerable charge on a dielectric. A small Marx generator (250 kilovolts) is available and may be used in the program. These voltages are extremely dangerous and may negate the use of the generator. Such an addition will require caution and slight chamber modification.

The RF characteristics of triboelectric charging and associated discharges are readily affected by the uniformity of the charging particle stream, particle velocity, length of path of physical contact between the charging particle and the dielectric material, the length an arc must jump to ground, or the proximity of the discharge to the radiating metal structure, humidity and some others as yet unidentified.

The sample is placed in a clamp that can be adjusted in three axes allowing the stream of charging particles to hit the sample at angles of incidence from 0° to 60° . An examination of any highspeed aircraft will show that practically all particle-surface contact will take place in this range.

An electrooptical targeting system is employed to constantly align the sample and the particle source. A H-62 photo duo-diode (Texas Instruments) is used in the pointing system. Its diameter is only 0.010 inch. Therefore, the narrow beamwidth provides an extremely accurate pointing system. Accuracy on the order of $1-2^\circ$ is easily obtained. Such an arrangement allows the operator to direct the charging blast directly in the middle or at any preselected spot on the target with a high degree of repeatability.

Monitoring leads are provided to the outside for observing the charging current, number of particle impacts and/or discharges per second or any convenient interval, DC potential of the sample, amplitude and waveform of the impact and discharge pulses, and effect upon the selected receiving circuitry. Ambient humidity is also noted.

This facility is located indoors. The dielectric discharges are subject to numerous reflections, and erroneous data are easily produced. Reflections (external to the chamber) are eliminated by completely enclosing the Plexiglas cage with two layers of Eccosorb FL 330. This particular absorbing material is good down to 2300 MHz. Variations in received signal strength of 1-2 db at 1000 MHz are produced by someone walking around the chamber. Such a small variation can be ignored in a random process like triboelectric charging. Reflections from the interior surface of the funnel are more difficult to control. They are calibrated out of the system for each sample at every frequency of interest by noting the total losses (radiating portion of dielectric sample, free space, antenna, and interconnecting cables) incurred. These data were used in preparation of the figures depicting the RF signal strength on the surface of the sample.

Along with the many good features of this facility, there are admittedly a few areas that could stand improvement.

During normal operation part of the charging, particles are directed back toward the operator producing a voltage of 500 volts on the surface of the chamber. The charged area is not in the operator's normal area of work and presents no danger; however, it must be remembered for safety's sake.

Reckless operation of the spray gun is neither recommended nor tolerated. A direct blast of flour at 18 inches will charge the Plexiglas to 25+ kilovolts. Experiments on a previous chamber indicated a voltage of 5+ kilovolts remained after 30 minutes. Charged areas can easily be recognized. The charging particles will settle on the interior surfaces in patterns which show the distribution and magnitude of the voltage.

The degree of air tightness is essential in order to keep possible explosive mixtures of powder/air confined away from furnace pilot lights etc., to keep the surrounding work area clean, and to provide a reasonably constant environment. If charging blasts longer than 2 seconds are used, the internal air pressure actually pushes the air gun out of the chamber. For longer blasts (2-4 seconds), the operator cannot maintain a steady source position; instead, he will be 1-2 inches further away from the sample.

One major auxiliary subsystem is necessary for operation, i.e., the air system. The present air system places 0-40 PSI on the container holding the charging particles. These particles are then injected into a 100-PSI stream of air. The spray pattern may be altered by using different nozzle configurations. For our purposes, a 0.086-inch diameter nozzle is used. The humidity of the active air stream is not monitored. A dry compressed air system is prohibitive, particularly from the cost standpoint.

Humidity may be a problem but its magnitude is unknown. A search of available literature revealed the data shown in Figure 3 which shows the percentage correction factor for breakdown voltage versus relative humidity at 24°C (Reference 3). A 1/50 pulse has a rise time of 1 microsecond and a fall time of 50 microseconds. This nomenclature is generally accepted by high voltage impulse specialists. The 1/50 pulse voltage breakdown changes 16% while the relative humidity changes from 20% to 90%. A 16% change of peak voltage will correspond to a noise radiated level change of 2 db.

The observed pulse rise times taken across 50 ohms with a Tektronix 585 oscilloscope were approximately 4-16 nanoseconds (ns) with pulse widths on the order of 20-160 ns. The effect of humidity on these impulsive high voltage breakdowns is impossible to extrapolate from Figure 3. During these tests the ambient humidity was noted and varied from 5-40%. Tests confirmed that the ambient humidity was equal to that of the compressed air stream.

It must be remembered that relative humidity decreases with altitude. At operating altitude (above cloud level), the relative humidity is essentially 0%. Therefore, the preceding statements apply only to the conditions under which these tests were conducted.

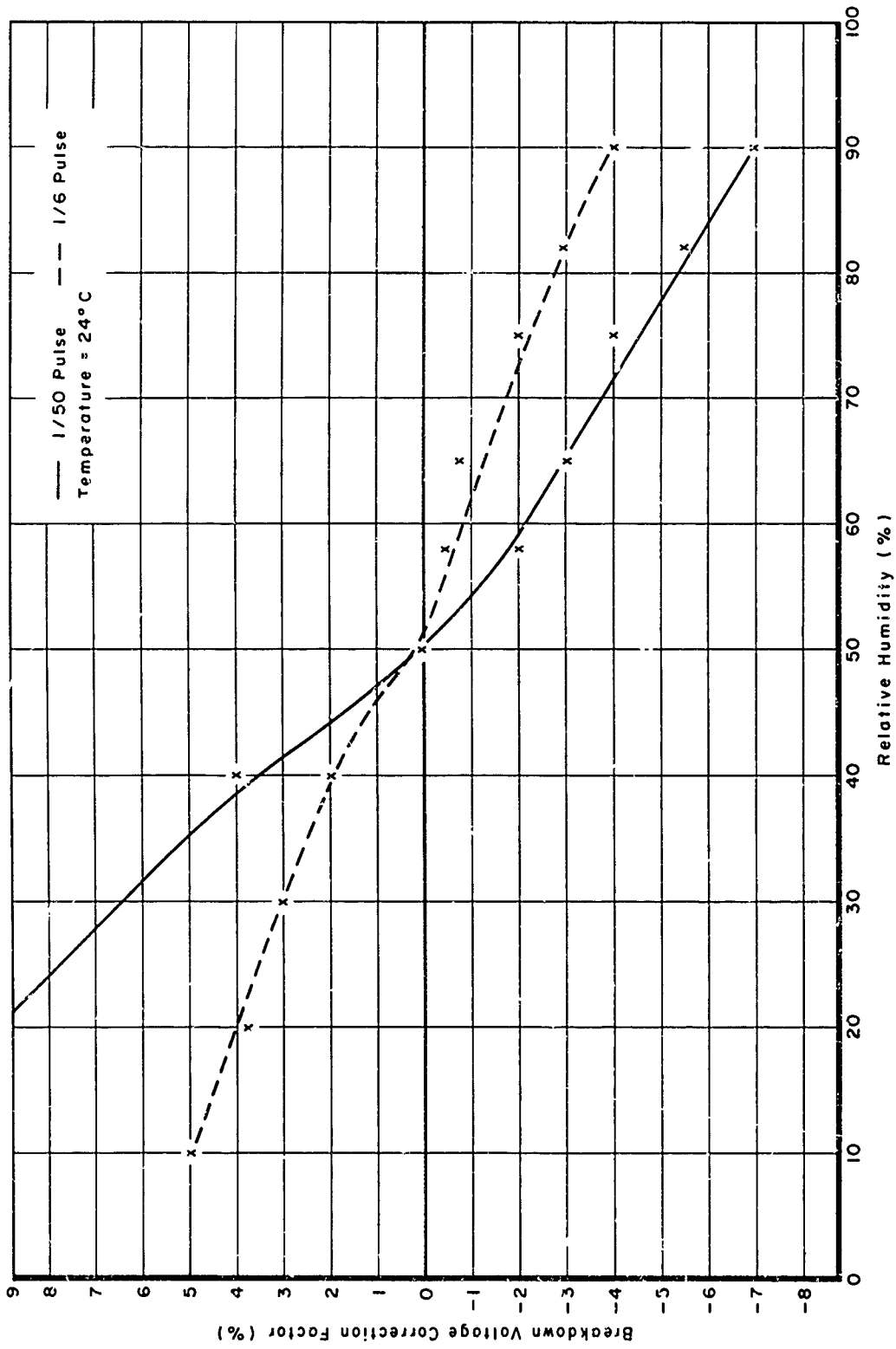


Figure 3. Breakdown Voltage Correction Factor Versus Relative Humidity

SECTION IV

TEST EQUIPMENT

The antenna system consisted of a conical log spiral covering the 1 GHz to 10 GHz frequency range and was operated in the far field region. When the noise is linearly polarized, this type of antenna will give readings 3 db low. This should not be of much concern for a random process like precipitation static.

For pulse observation, matched cables (from the sample to oscilloscope) and a high speed oscilloscope are essential. RG-9 cables were used and were adjusted for minimum distortion of a unit step input on the HP Time Domain Reflectometer. This particular instrument has a rise time of approximately 150 picoseconds (ps). A Tektronix 585 oscilloscope (90 MHz bandwidth) was used to observe these pulses.

During an investigation of this type, a question that usually arises is "What is the amount of the DC potential of the sample?" An electrostatic voltmeter is the ideal instrument to monitor the DC potential because of its extremely high input impedance. The following example will serve to illustrate how important this point is.

Sample voltage = 10 kilovolts

Voltmeter input impedance = 10 megohms

When Ohm's Law is used, $I = 1$ milliampere

A current of 1 milliampere may seem to be insignificant, however, this is not the case. A recent study on the CH-54 (Flying Crane) helicopter has shown that the triboelectric charging rate is 150 microamperes for loose dry snow in Alaska (Reference 4). The experimental samples are considerably smaller than a CH-54, therefore, the anticipated triboelectric charging currents will also be much less. The electrostatic voltmeter employed in these tests had a leakage resistance of at least 1×10^{15} ohms. This leakage resistance is the equivalent of input impedance. Now the current drawn from a 10-kilovolt source is 10×10^{-12} amperes, a completely negligible current. Ordinary high resistance will not work. A resistance of 1000 megohms will reduce the peak voltage by a factor of 4.

An estimate of the current magnitude to be measured may be obtained as follows. Flight tests reveal that a charging rate of 1-30 microamperes/ft² can be expected when ice crystals are the charging medium (References 1 and 5). For the sake of uniformity and ease of comparing results, an attempt was made to maintain a constant sample size (2 1/2 inches by 5 1/2 inches). The expected charging current can now be computed to be approximately 1-3 microamperes. A HP 425A DC microvolt-ammeter with a full scale sensitivity of 10 picoamperes was used to monitor the charging current. Two major problems are presented when an instrument of this type is used. First, the impedance is very low as shown in Table I.

TABLE I
HP 425A INPUT RESISTANCE

Microampere Range	Input Resistance (ohms)
1	500
3	333
10	100
30	33

When the current is being monitored, the other instrumentation will not work properly due primarily to the small load placed across the RF noise source. A DC current is being measured from an AC source, therefore, very little can be said about peak currents. These measurements were performed for qualitative measurements only.

A Polarad microwave receiver (Model R) was used as the received signal indicator. This receiver has three display scales: two are logarithmic and the other is linear. These pulses were so fast that the receiver operated in the linear mode all the time. Also, it was not optimized for pulse reception. Therefore, a pulse calibration was performed. The receiver read approximately 25 db low on pulses encountered in this study.

SECTION V
SYSTEM CALIBRATION

One very important variable is particle velocity. What is it and is it constant? The second portion of the question is easily minimized by keeping the source to sample distance relatively constant. The other portion takes a little work. A method of measurement was used that employed two electrodes, an attenuator and a memoscope. The electrode nearest the spray gun was called the trigger electrode. It intercepted about 50% of the charging stream and was connected to the memoscope's external trigger through a 20-db attenuator. The amplitude electrode was downstream 1 1/4 inches to 8 inches and intercepted the remainder of the charging stream. This electrode provided the vertical input of the scope. A standard pressure of 100 PSI was used in the airstream and 45 PSI was maintained on the particle storage can. These pressures produce an emerging air stream velocity of 3900 ft/sec. Figure 4 shows the computed velocities and Table II lists the standard deviations.

TABLE II

PARTICLE VELOCITY STANDARD DEVIATIONS

Source to Sample Distance (inches)	Standard Deviations
1.25	48
3	55
5	102

These standard deviations are about what one would expect because the computed times depend on the quickness with which the air gun trigger is pressed, the amount of particles (flow) in the air gun container, and external influences such as cross or opposing air currents. These tests were conducted outside the test chamber, and air currents may have been a major factor in determining the accuracies at the 5-inch distance.

During these velocity measurements, some uncertainty arose concerning the start of the horizontal sweep of the memoscope. A typical sweep is shown in Figure 5.

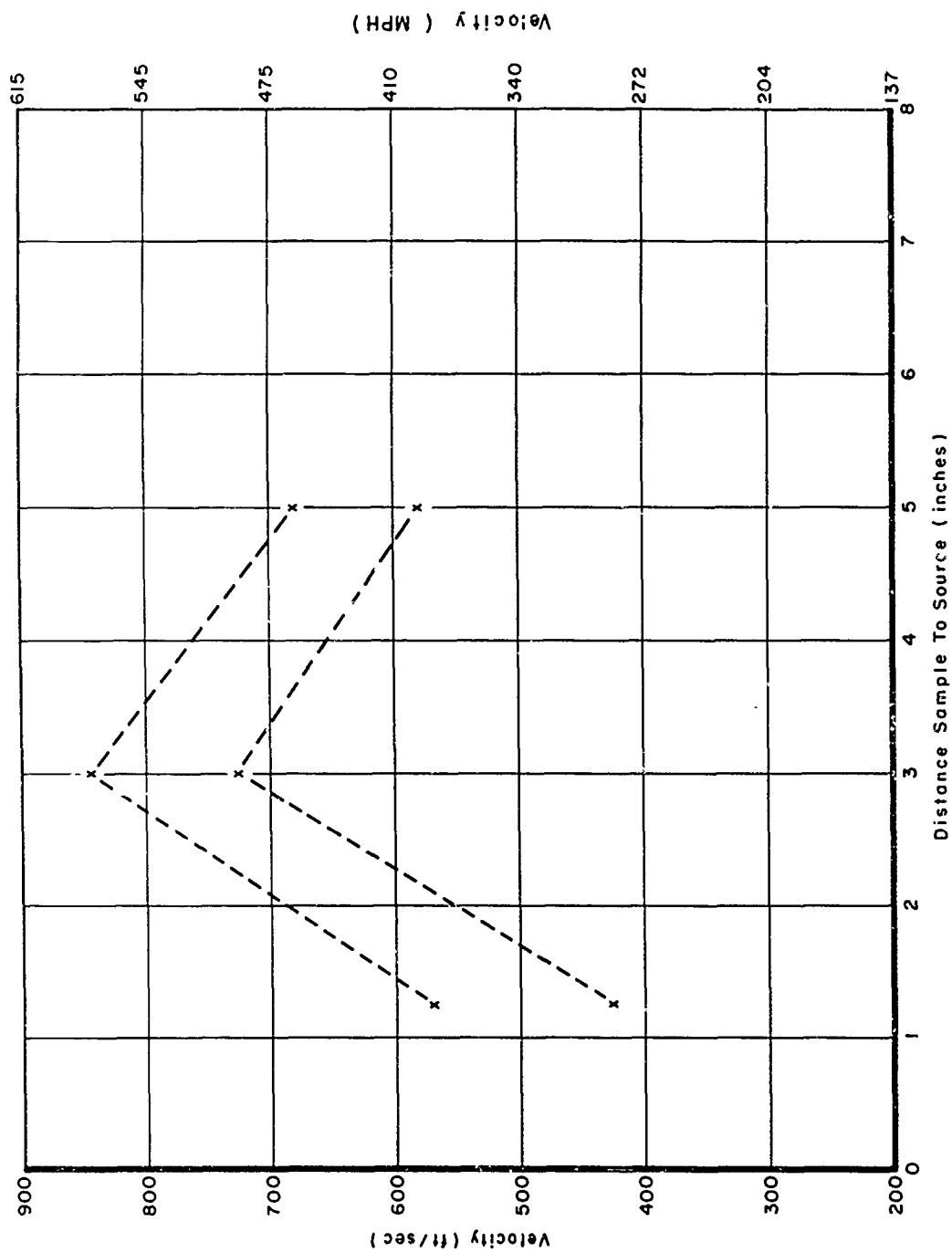


Figure 4. Range of Computed Stream Velocities

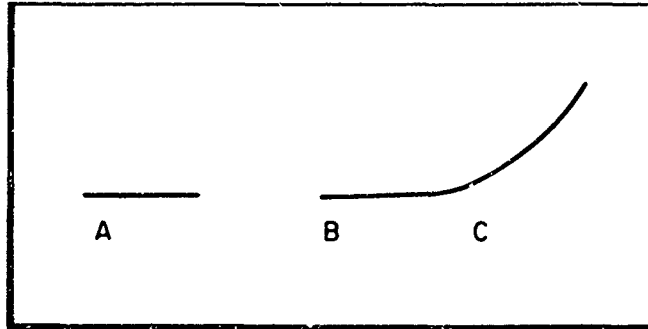


Figure 5. Typical Memoscope Trace

The particles definitely began to reach the amplitude electrode at C. A gap in all traces occurred between A and B, giving rise to the uncertainty in the particle velocity computation. If we take the mean between the upper and lower bounds (Figure 4), we obtain velocities of approximately 345, 520, and 440 MPH. These values are reasonable approximations to the actual velocities.

Received signal strength will depend on the polarization characteristics of the transmitter and receiving antennas and reflections, both external and internal. Assuming a worst case condition where the signal is randomly linearly polarized and reflections are randomly present, the total measurement error due to these two factors is

$$\sqrt{(0.5)^2 + (0.65)^2} = 0.8$$

where 0.5 = power lost due to linear-circular polarization mismatch

0.65 = power lost due to random external reflection

Therefore, only 20% of the power will not be intercepted resulting in a loss of 0.97 db. A small figure may be of significant value if the signals are of very small amplitudes. For the most part, it can reasonably be ignored. Internal reflections were not measured but were considered as described below.

All samples had a closed copper or aluminum ring on the surface at the extremities for the purpose of radiating the RF energy of the streamers.

The radiating structure suffered numerous reflections from the interior of the test chamber due to the proximity of the funnel's large metallic surface. Each sample possessed different dielectric constants which in turn further modified the radiating properties of the metallic ring. The following procedure was employed to attempt to take these variations into account in the data reduction stage of the program. A CW signal generator was connected to the ring through a 20-megohm resistor. The large resistor was used to isolate the generator from the ring. A known level of power was transmitted at each frequency and the received power was measured. This method gave the total loss between the generator output connector and the receiver input. Variations of loss with respect to frequency ranged from 41-77 db.

In order to establish a baseline for optical pulse evaluation, a TEK 111 Pretrigger Pulse Generator was used to produce 2-ns pulses with a rise time of less than 0.5 ns. This signal was used in a matched configuration (line adjusted for minimum impedance variation) to obtain the response of the oscilloscope and its vertical plug-in. Photographs were made of the scope display during all of these system calibration measurements.

The photos were extremely valuable when small changes were made in the coaxial lines. After the rise-time characteristics of the scope and its cabling system are determined, one can determine the minimum observable rise time and its accuracy as follows:

$$t_{R \text{ min}} = \sqrt{(t_{RC})^2 + (t_{RP})^2 + (t_{RO})^2}$$

$$t_{R \text{ min}} = \sqrt{.25 + 2.25 + 15.35 \times 10^{-18}} = 4.22 \text{ ns}$$

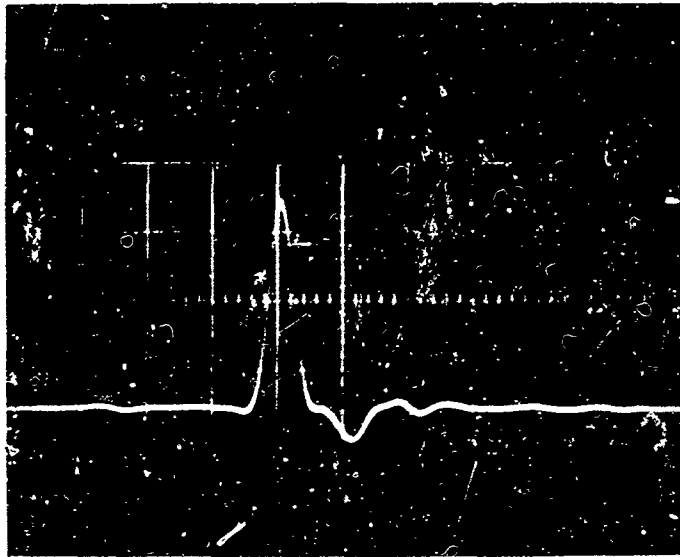
where

$$t_{RC} = \text{rise time of cable 10 ft of RG-9} = 0.5 \text{ ns}$$

$$t_{RP} = \text{rise time of main scope plug-in} = 1.5 \text{ ns}$$

$$t_{RO} = \text{rise time of main scope vertical amplifier} = 3.9 \text{ ns}$$

If the cable rise time is eliminated, the resultant minimum observable rise time is 4.2 ns. This is confirmed in Figure 6, which shows the system's impulse response with an Empire Devices IG-118 impulse generator (1-10 GHz) as the signal source.



time scale = 10 ns/cm

Figure 6. Impulse Response

What is the observed accuracy of the system when observing step functions of microsecond and nanosecond rise times? We must use the same technique as outlined above. A sample calculation is now presented.

$$t_{R \text{ min}} = 4.2 \text{ ns (calculated previously)}$$

$$\text{step function } t_R = 4 \text{ ns}$$

$$\text{observed } t_R = \sqrt{(4.2^2 + 4^2) \times 10^{-18}} = 5.8 \text{ ns}$$

$$\text{error} = 45.0\%$$

The errors for step functions of various rise times are tabulated in Table III. The purpose of this exercise is to establish the limits of the measuring system. Therefore, if pulses with rise time 4x greater than the system limit are observed, we can be sure that the observed pulses are not distorted by the cabling or oscilloscope; 15 ns rise times will be observed as 15.5 ns resulting in an error of -3.3%.

Once the pulse rise times and widths are determined for each sample, the receiver may be calibrated as follows. A pulse generator producing a substitute equivalent pulse is connected to the receiver. Its repetition rate is controlled by the oscilloscope sweep timing circuit. The repetition rate is varied from single

TABLE III
OBSERVED RISE-TIME ERRORS

Step Rise Time (ns)	Observed Rise Time (ns)	Error (%)
2.0	4.65	+ 232
3.0	5.17	+ 72.5
4.0	5.8	+ 45.0
6.0	7.32	+ 18.9
8.0	9.05	+ 13.1
10.0	10.8	+ 8.0
15.0	15.5	+ 3.3

pulses to repetition rates such that any further increase will not result in an increase of indicated received power. Tests indicated that the receiver readings during the experiments would be 20-30 db low. Table IV illustrates how serious this problem can be.

TABLE IV
RECEIVER PULSE RESPONSE

Pulses/Sec	Indicated Received Power (dbm)
1	-62
5	-57
10	-50
100	-40
1000	-40
adjusted for peak value	-34
Pulse: rise time 2 ns Pulse width = 20 ns Receiver frequency = 1 GHz	

This calibration is absolutely necessary for radiation readings produced by precipitation static because only the larger pulses will possess enough energy to overcome losses of 41-77 db and still be registered as a noise pulse by the receiver. Furthermore, the frequency of occurrence of these pulses is about 1/1000 that of the pulses counted by the frequency counter when it is connected directly to the sample. Thus one cannot go from making conducted to radiated measurements without taking this repetition rate difference and its effect on the receiver's circuits into account.

SECTION VI

TEST SAMPLES

The following materials were examined for precipitation static properties:

1. Quartz
2. Teflon
3. Epoxy
4. Epoxy honeycomb section from an operational aircraft
5. Epoxy laminate nose cone from an operational missile
6. Acrylic (Plexiglas)
7. Alumina
8. Slotted metallic RF window (SMRFW)--Reference 6: An RF transparent device composed of dielectric backed perforated metallic sheet; referred to as SMRFW(A) and SMRFW(B) in Figure 8.
9. Polyester-coated slotted metallic RF window (Selectron 5063 resin cured with benzol peroxide): Referrred to as polyester-coated SMRFW(B).

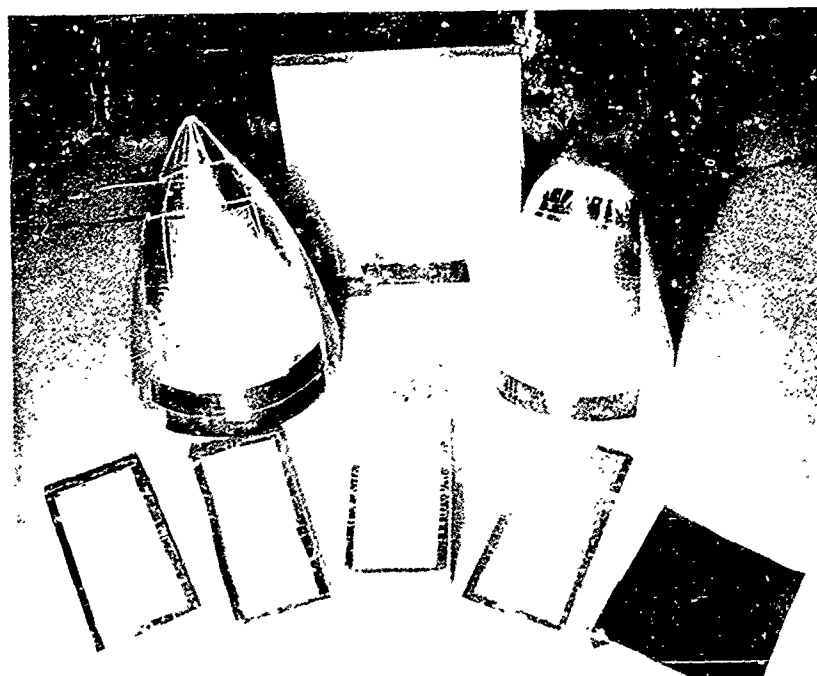
10. Polyester-coated slotted metallic RF window with metallic layer grounded

11. Copper (a standard for measuring impact noise)

For the sake of uniformity, an effort was made to obtain all samples in 3-inch by 6-inch flat sheets. This was done on Samples 2, 3, 4, 6, 8, 9, and 10. No. 11 had the same area as the flat sheets. Samples 5 and 7 were three-dimensional shapes similar to an ogive. The piece of quartz was approximately 8 inches by 8 inches. A copper or aluminum ring (2-1/2 inches by 5-1/4 inches) of conductive tape was placed on all samples and enclosed the testing area. The excess area was covered with conductive tape in order to maintain a constant test area on all shapes. Samples are shown in Figure 7 and 8.

These particular materials were chosen because they are currently used on aircraft or because they show promise for future application. Quartz and acrylic are presently used for optical windows; Teflon and epoxy laminates are used for fuselage sections and alumina is used as a high temperature dielectric. The slotted metallic RF window is the result of an AFAL-sponsored program to design an antenna covering to reduce precipitation static and catastrophic damage due to lightning.

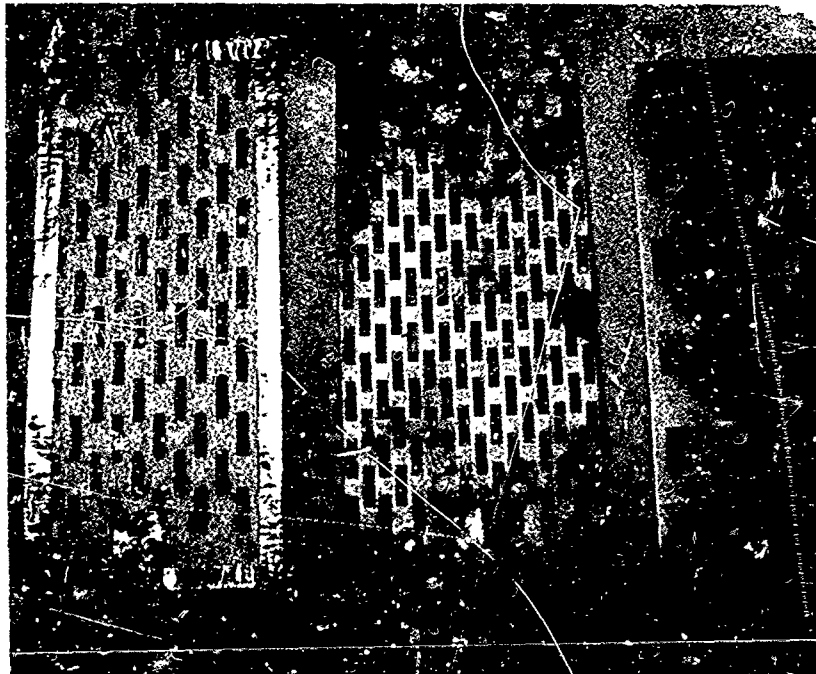
As a point of reference, the applicable physical constants as obtained from various chemical and physics handbooks (References 7 through 13) are listed in Table V. No effort was expended to chemically clean the dielectric surfaces. In actual service the surfaces would probably be contaminated. The stream of charging particles would also serve to abrade the contaminating body oils (fingerprints).



Back Row Left to Right: Missile Nose Cone, Quartz, and Alumina Nose Cone

Front Row Left to Right: Teflon, Plexiglas, Fuselage Section of Operational Aircraft, Epoxy, and Copper

Figure 7. Test Samples



Left to Right: Polyester-Coated SMRFW(B),
SMRFW(B), and SMRFW(A)

Figure 8. Slotted Metallic RF Window Samples

TABLE V
PHYSICAL CONSTANTS

Sample	Volume Resistivity (ohm-cm)	Dielectric Strength (V/Mil)	Dielectric Constant	Dissipation Factor	Arc Resistance* (arc seconds)	Coefficient of Thermal Expansion $\left[\frac{\text{in}}{\text{in}}(\text{C}^\circ) \times 10^{-5}\right]$
Epoxy	10^{16} - 10^{17}	300-400	3.5-5.0 at 1 MHz	.01 at 1 MHz	120-190	1.1-5.0
Alumina	10^{11} - 10^{14}	230	9.4 at 1 MHz	.0001 at 1 MHz		7.1×10^{-1}
Acrylic	10^{14} - 10^{15}	400	3.3-3.9 at 60 Hz	.04-.05 at 60 Hz	no tracking	6.5-10.5
Teflon	$> 10^{18}$	400	2.1 at 60 Hz	$< .001$ at 60 Hz	no tracking	5.5
Quartz	$> 10^{19}$		3.75-4.1 at 100 MHz	.001 at 100 MHz		5.7×10^{-2}

*Arc Resistance: a measure of an electrical breakdown condition along an insulating surface, caused by the formation of a conductive path on the surface.

SECTION VII
SAMPLE POSITIONING

During a portion of the testing program, the samples were placed in open space at an angle of 45° with respect to the charging stream. The coupling factor was obtained by connecting a signal generator to the ring through an isolation resistor. This method is referred to as Method A.

A ground plane (17 inches by 17 inches) was constructed with a hole in the center to receive the samples. Isolation was maintained between the ground plane and the sample. The coupling factor was obtained by exciting a short stub (1/4 inch) on the end of a shielded isolation resistor. This resistor assembly was rigidly fixed in place during testing and calibration in order to eliminate another sticky variable. The 1/4-inch dimension was chosen so that it would be a small fraction of a wavelength over the frequency range of interest. A distance of 1/8 inch separated the stub and the radiating device at all times. On the epoxy sample the coupling factors varied from 54 to 69 db (81% in the low 60s), demonstrating a reasonable amount of frequency independence with respect to the radiating structure. Use of the ground plane is referred to as Method B.

Coupling factors were measured for each sample even if the dimensions were the same. This extra measure accounted for slight displacements in the holding assembly, sample curvature, and possible external reflections.

Obtaining coupling factors at 140 kilohertz required a modification of the former procedure. The isolation resistor had to be connected directly to the radiating structure due to the extreme inefficiency of using a radiator of 3×10^{-5} wavelengths to excite the secondary radiator. No great precision was attempted concerning the results at 140 kilohertz. These tests were used as a low frequency back-up in an effort to explain the strange results observed at microwave frequencies.

SECTION VIII

RESULTS

For uniformity, all figures were computed with the least squares technique unless specifically stated.

The computed generated signal strengths (S_{db}) using data provided by mounting Method A are illustrated in Figure 9; i. e., mounted in free space with no ground plane. Applicable line equations are given in Table VI.

TABLE VI
LINE EQUATIONS FOR FIGURE 9

Teflon	$S_{db} = 119$
Epoxy	$S_{db} = 119.5 + 0.7 f_{GHz}$
Quartz	$S_{db} = 119.5 - 1.6 f_{GHz}$
Acrylic	$S_{db} = 102.4 - 1.6 f_{GHz}$
Alumina	$S_{db} = 100.7 - 2 f_{GHz}$
Aircraft Sample	$S_{db} = 113.2 - 0.5 f_{GHz}$
Missile Nose Cone	$S_{db} = 78$
SMRFW(A)	$S_{db} = 108.2 - 3.2 f_{GHz}$

Note the shallow slope or its complete absence. This could possibly be due to the operator subconsciously "pushing" the sample to obtain readings; however, a check of the records indicated that this was not so. The cutoffs for the SMRFW(A), acrylic, and alumina samples were actually observed. A check of receiver sensitivity indicated no system malfunction existed. Further calculations show the minimum observable signal at the next frequency to be more than adequate for reception. The major point of interest in this figure is the relative noise levels. These tests were conducted on the same day.

The average received signal provided by mounting the samples on the ground plane, Mounting Method B, are shown in Figure 10. Here the relative

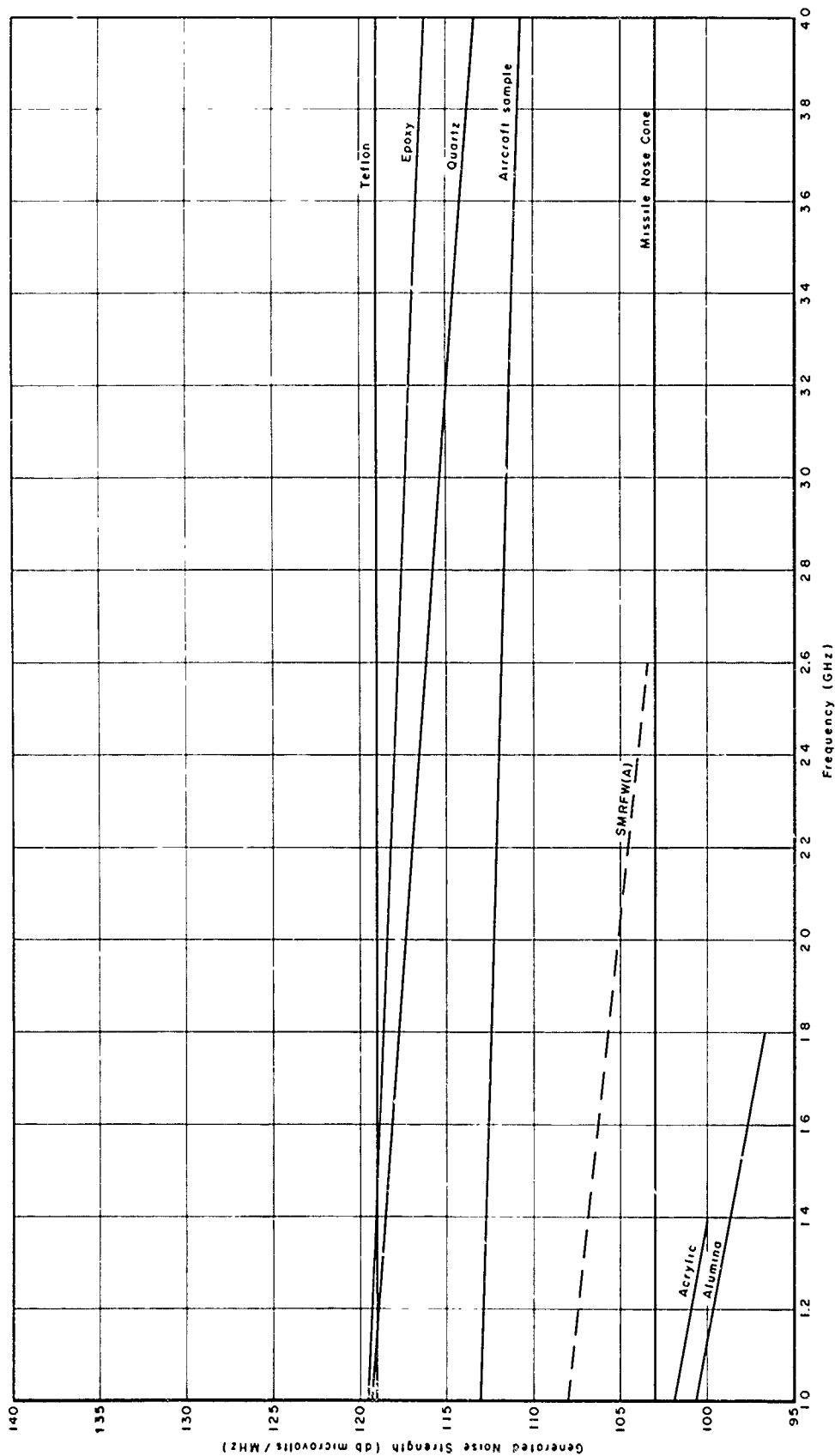


Figure 9. Computed Generated Signal Strengths (Mounting Method A)

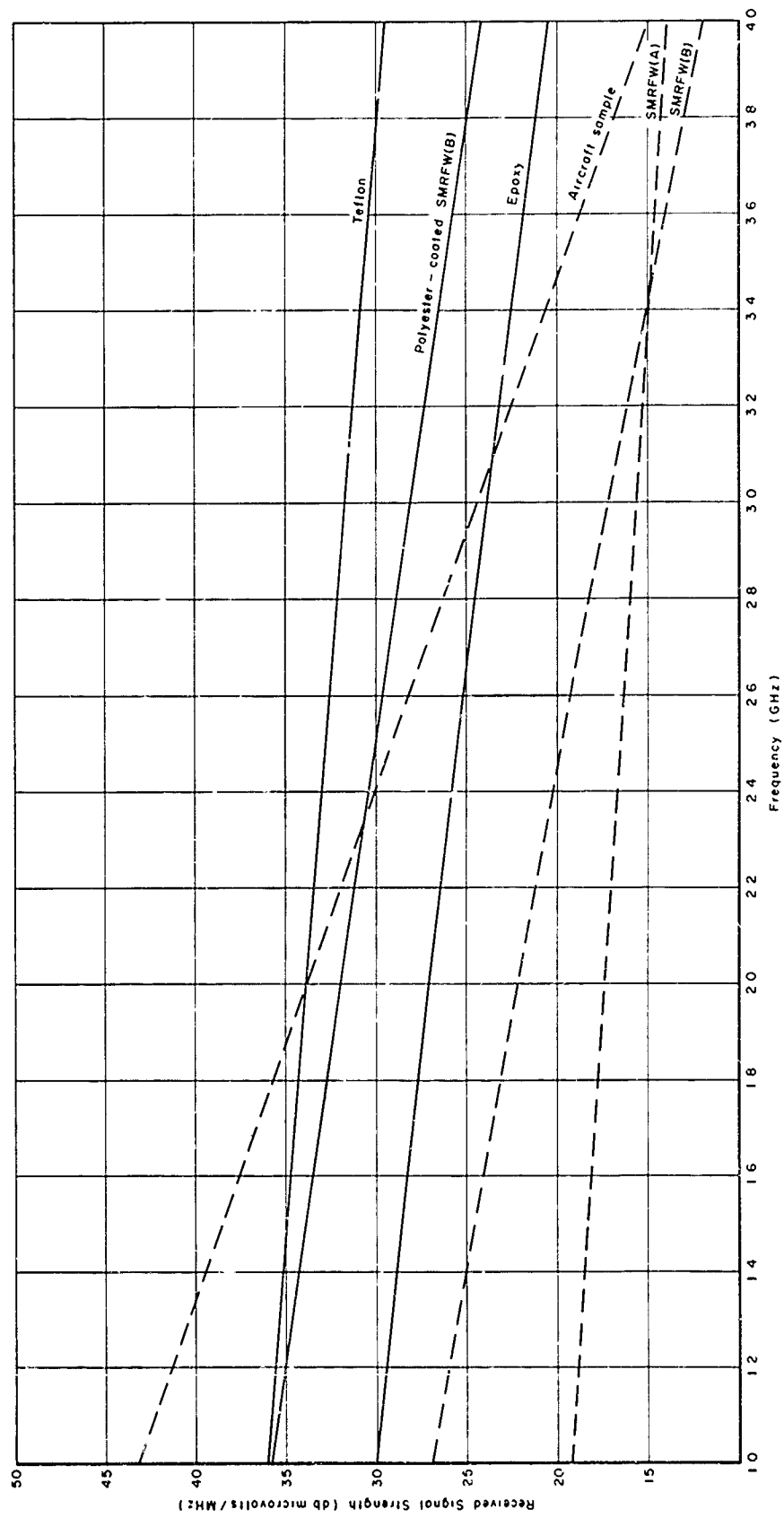


Figure 10. Average Received Signal Strength (Mounting Method B)

levels and slopes are readily evident. Incorporation of the coupling factors and pulse correction yield the results shown in Figure 11. Comparison of these two figures illustrates the importance of determining the coupling factor every time a sample is used (note the relative positions and slopes). Again this series of tests was conducted on the same day using only samples that would be used to cover antennas. In actual practice, the SMRFB(B) metallic portion of the polyester-coated SMRFB(B) sandwich would be grounded to the airframe. The appropriate line equations for Figure 11 are listed in Table VII

TABLE VII
LINE EQUATIONS FOR FIGURE 11

Polyester-coated SMRFB(B)	$S_{db} = 133.6 - 5.05 f_{GHz}$
Teflon	$S_{db} = 130.7 - 4.85 f_{GHz}$
SMRFB(B)	$S_{db} = 120.6 - 4.25 f_{GHz}$
Epoxy	$S_{db} = 116.3 - 1.32 f_{GHz}$
Aircraft sample	$S_{db} = 126.8 - 5.5 f_{GHz}$
SMRFB(A)	$S_{db} = 117 - 4.4 f_{GHz}$

The equations for a number of tests on various samples under the free space and ground plane method of positioning are listed in Table VIII. A wide range of initial levels at 1 GHz and slopes is apparent.

The signal strength envelopes for multiple tests on selected samples are shown in Figure 12. As a result of the large variations, it is evident that these figures only illustrate approximate signal levels. Therefore, they are not to be taken as absolute values, average or maximum noise levels.

As a point of interest, the data presented in Figure 11 is used in Figure 13 and illustrates the noise levels relative to that produced by the aircraft sample. Its main purpose is to give the reader a recognizable point of reference.

Photographs of the pulse rise times were taken in order to calculate what the observed spectrum should be and to make a comparison between it and the experimental values illustrated in Figure 14 through 18. The photographs were

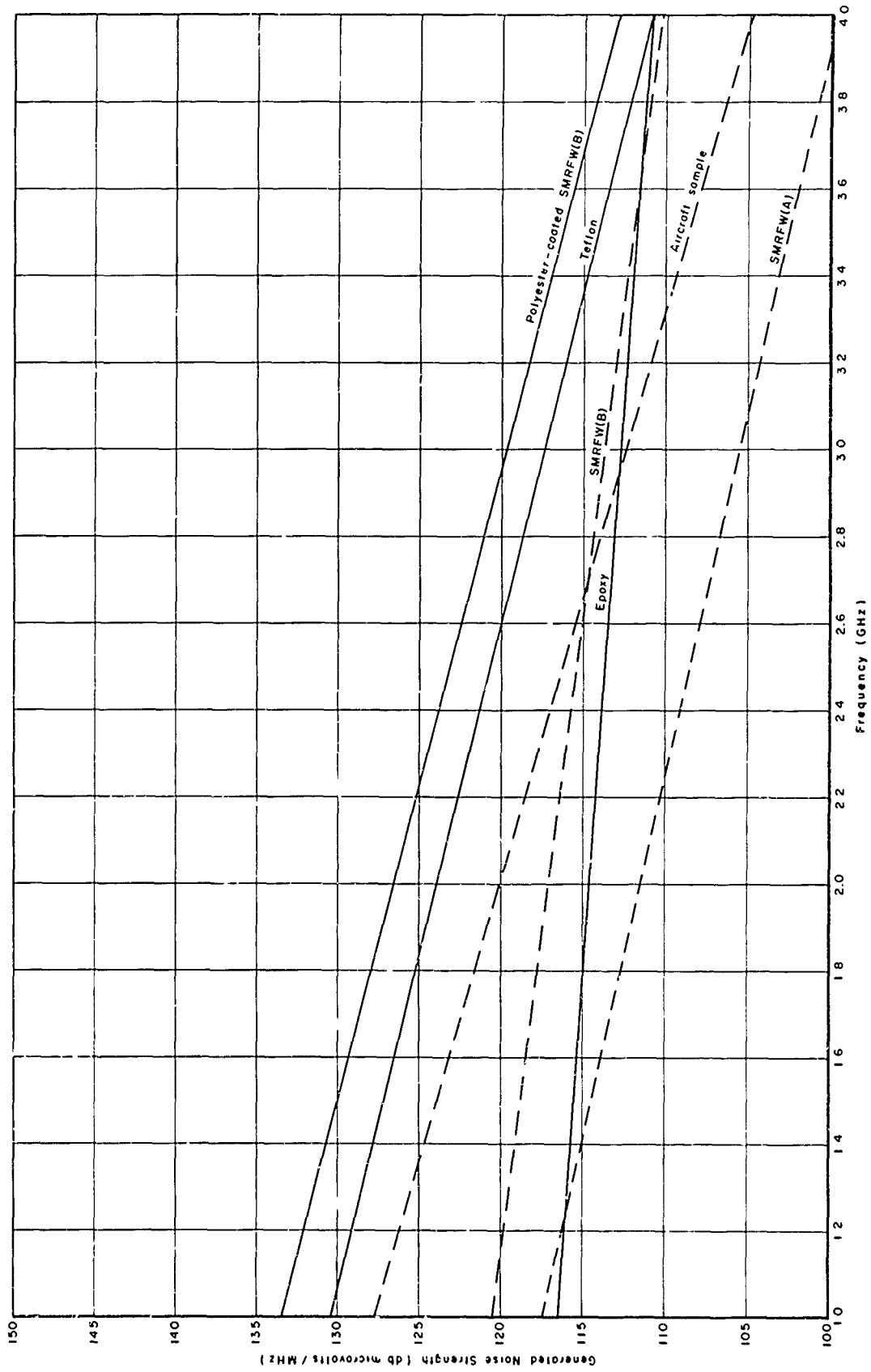


Figure 11. Computed Generated Signal Strengths (Mounting Method B)

TABLE VIII
COMPARATIVE READINGS

Aircraft Sample	111.3 + f* 113.2 - 0.5f 126.8 - 5.5f
Epoxy	118.7 - 4.6f 119.5 + 0.7f 116.3 - 1.32f
Teflon	106.7 - 1.5f 116 130.7 - 4.85f
Quartz	125 - 6f 119.5 - 1.6f
SMRFW(A)	108.2 - 3.2f stop at 2.6 GHz
Acrylic	102.4 - 1.6f stop at 1.4 GHz
Alumina	100.7 - 2f stop at 1.8 GHz
Missile	103
SMRFW(B)	120.6 - 4.25f
Polyester-coated SMRFW(B)	133.6 - 5.05f
* f = frequency GHz	

made with Polaroid 410 film (ASA 10,000 speed) at sweep speeds of 20 ns/cm. A picture with good contrast was difficult to obtain because of the fast sweep speed and low repetition rate.

The observed pulse parameters are listed in Table IX

Some interesting observations were made while these pictures were being taken. Figures 19 and 20 were taken of the aircraft sample at 50 ns/cm and 20 microseconds/cm, respectively.

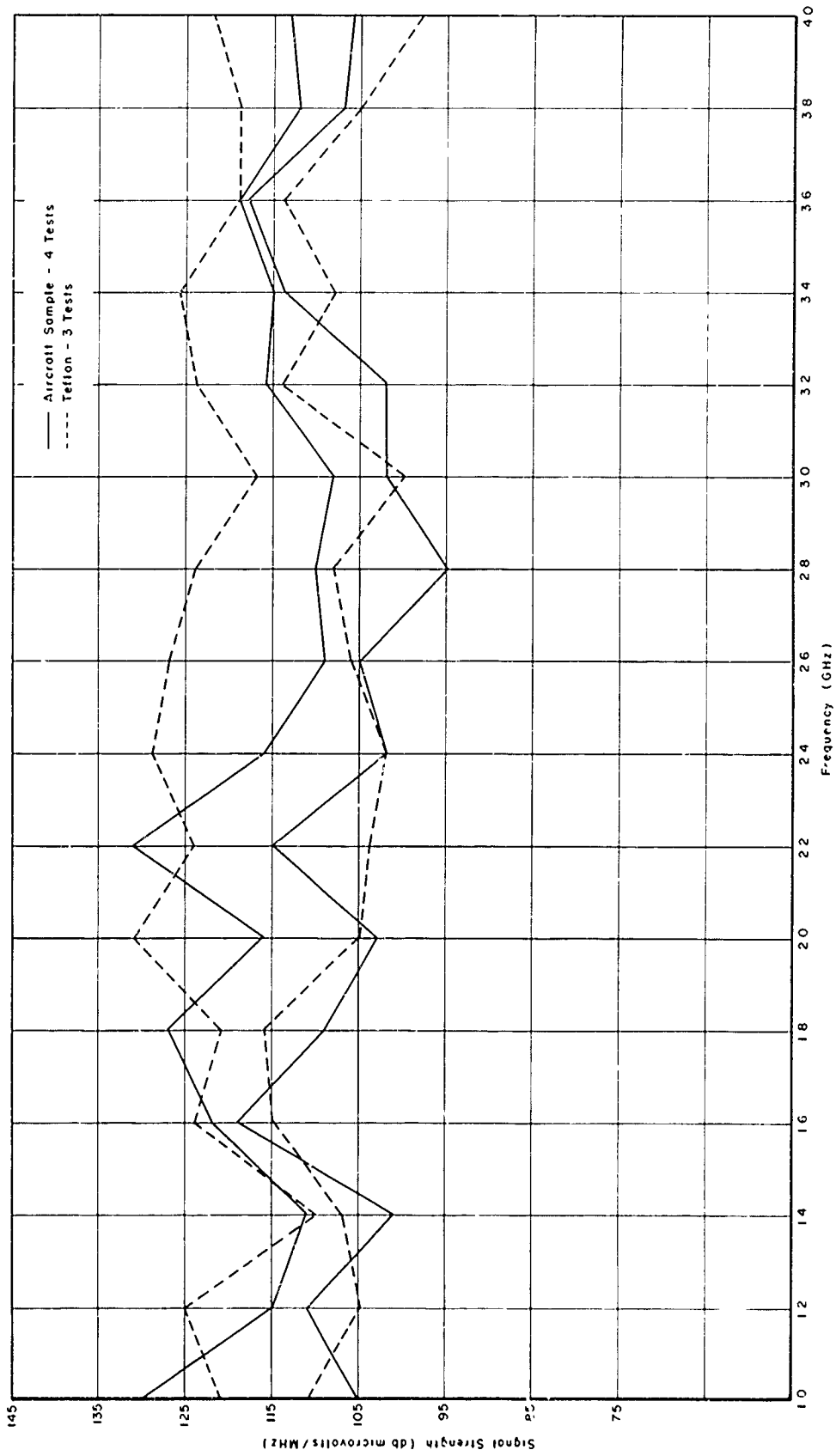


Figure 12. Generated Signal Strength Envelopes

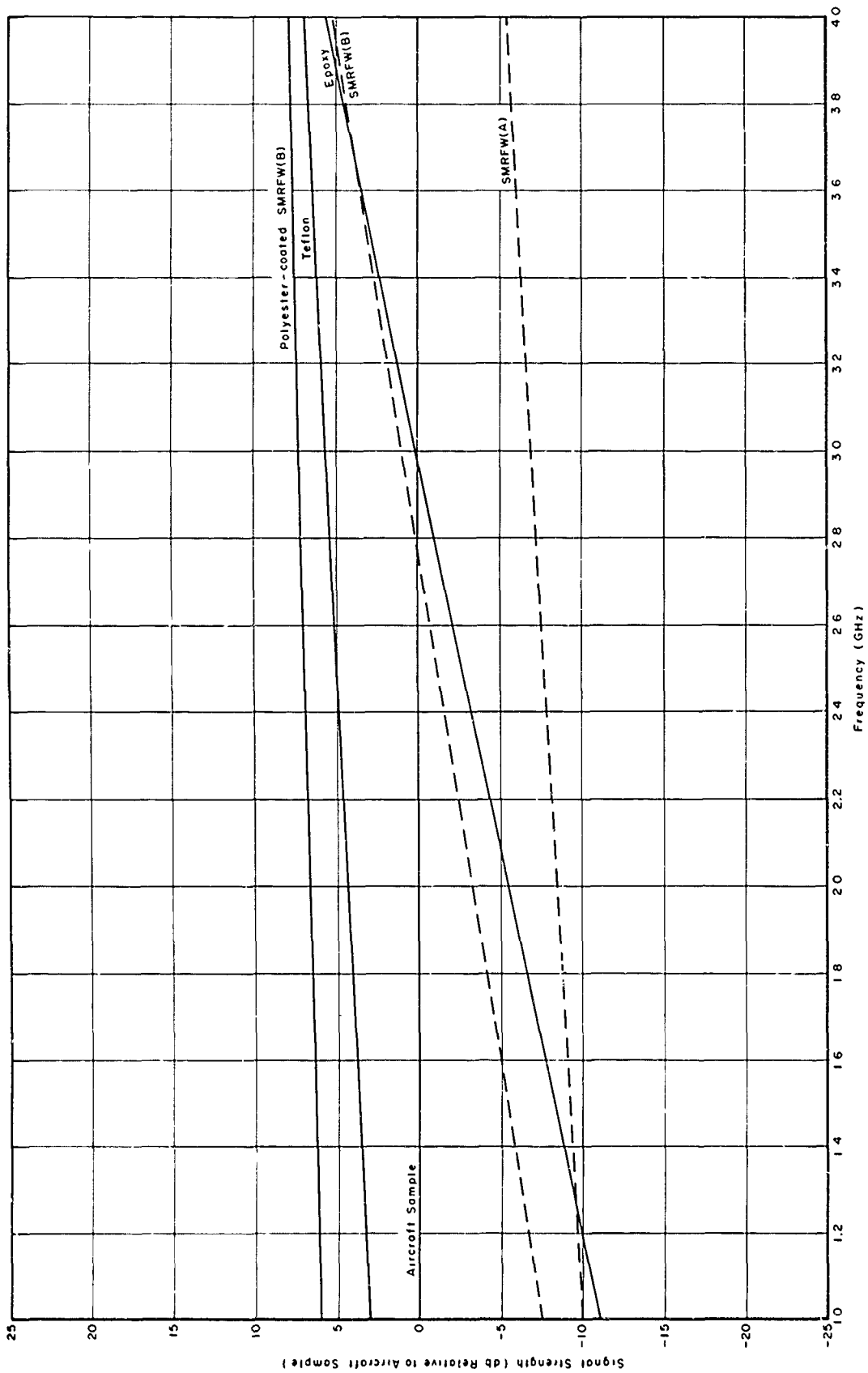


Figure 13. Noise Normalized to Aircraft Sample

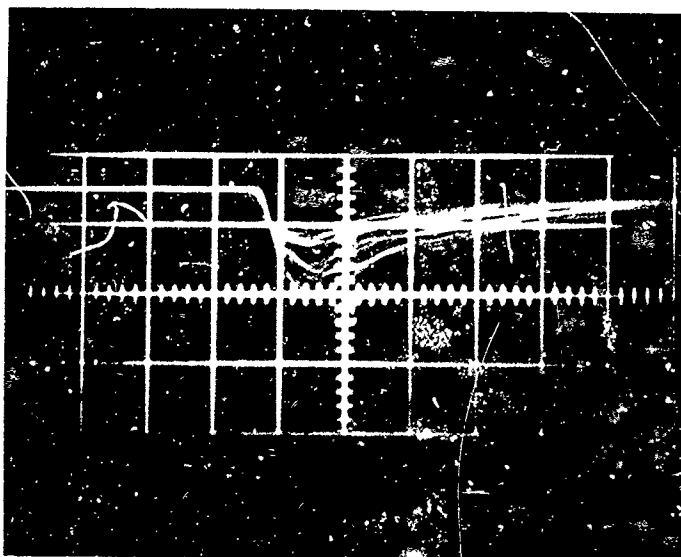


Figure 14. Teflon Pulses
Sweep speed = 20 ns/cm
Vertical scale = 0.5 volt/cm

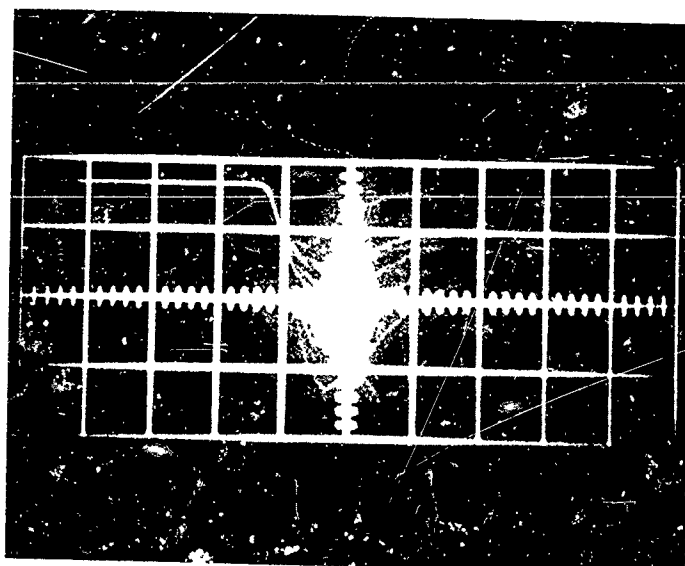


Figure 15. Plexiglas Pulses
Sweep speed = 20 ns/cm
Vertical scale = 1 volt/cm

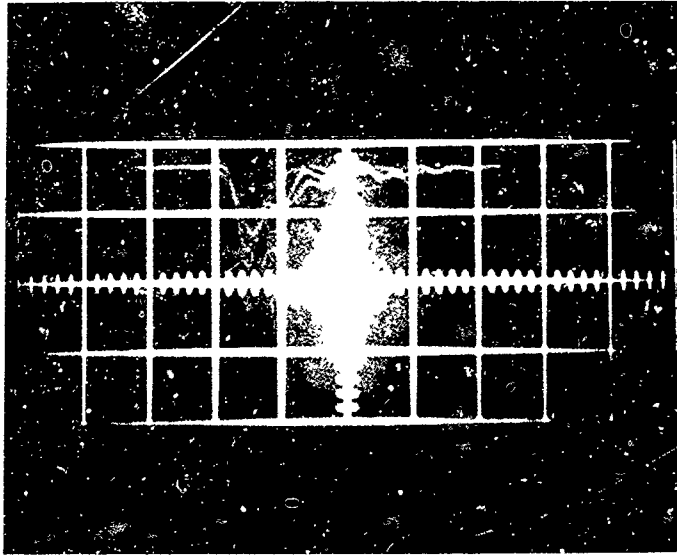


Figure 16. Polyester-Coated SMRFW(B) Pulses on Polyester Layer
Sweep speed = 20 ns/cm
Vertical scale = 0.02 volt/cm

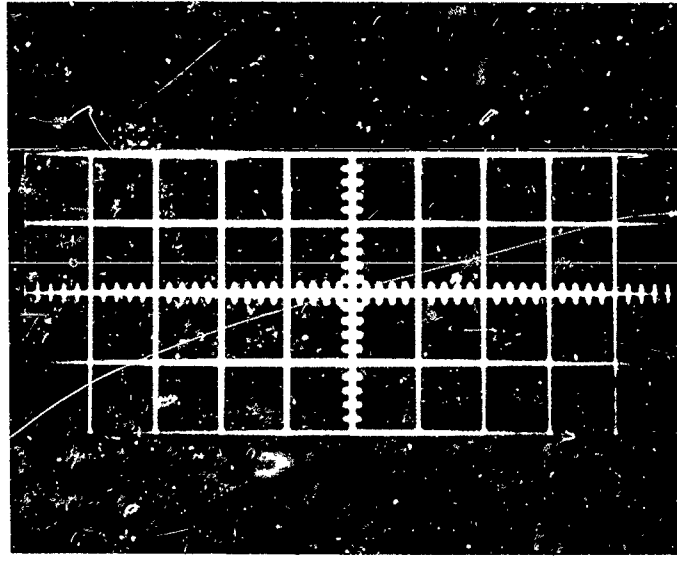


Figure 17. Polyester-Coated SMRFW(B) Pulses on Metal Layer
Sweep speed = 20 ns/cm
Vertical scale = 0.2 volt/cm

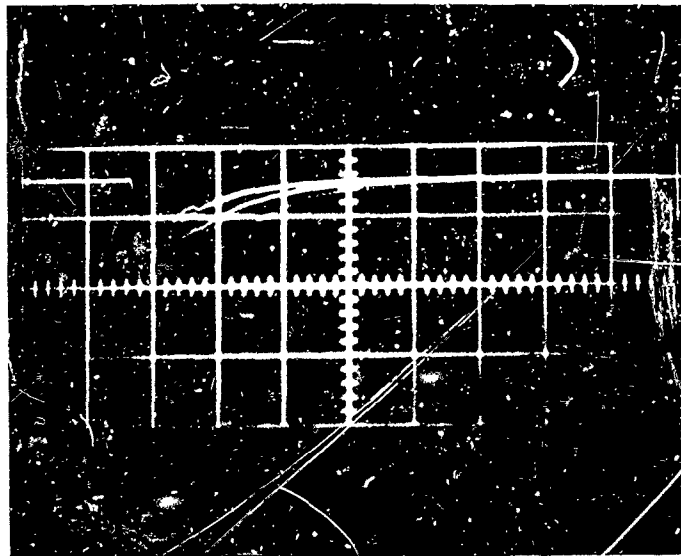


Figure 18. Epoxy Pulses
 Sweep speed = 50 ns/cm
 Vertical scale unknown

TABLE IX

PULSE PARAMETERS (ACROSS 50 OHMS)

Material	Rise Time (ns)	Width (ns)	Amplitude (volts)	Repetition Rate (pps)***
*Polyester-coated SMRFW(B)	6-12	20-120	.5	
**Polyester-coated SMRFW(B)	4	40	.04	120
Missile nose cone	12	100	.8	
Alumina	16	120	.6	20
Acrylic	12	120	3	40
Quartz	8	100	.6	120
Aircraft sample	8	100	3	40
Epoxy	8	150	2	
Teflon	16	120	1	

*Pulses reaching floating metallic layer
 **Pulses on polyester surface
 ***These rates are not detected by the receiver

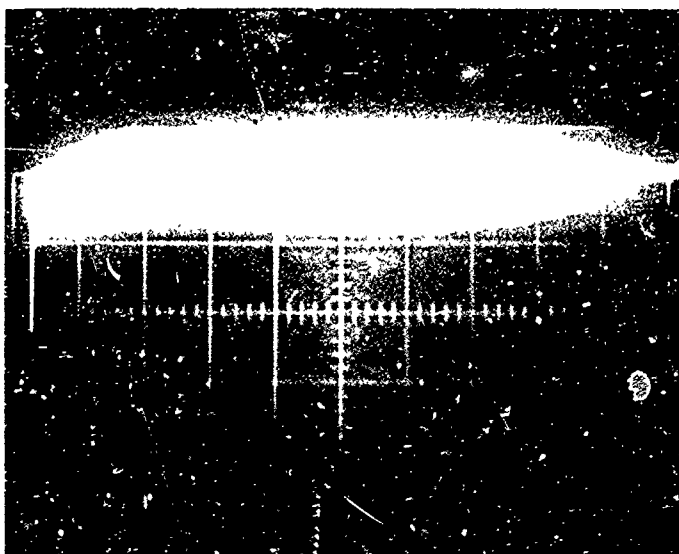


Figure 19. Aircraft Sample Pulse Train at 50 microseconds/cm

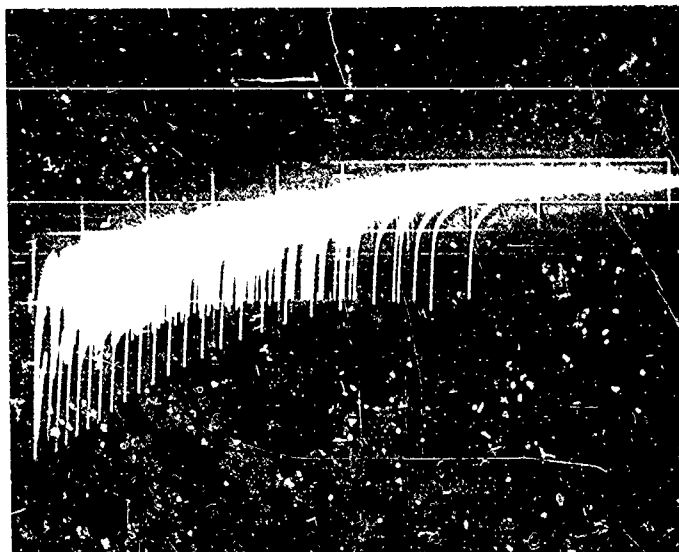


Figure 20. Aircraft Sample Pulse Train at 20 microseconds/cm

The structure of a single pulse composed of a primary pulse and many secondary discharges is shown in Figure 19. The time base is expanded in Figure 20. Two traces are apparent in this particular figure. The explanation for this behavior is as follows using Figure 21 as a guide. The potential at Point A is greater than those at the points marked B because of the nature of its position with respect to the metallic ring and the air-particle stream. An ionized path is produced by A discharging to the ring. Path resistance has now been reduced to approximately 5000 ohms (Reference 14); therefore, charges near the path see a much reduced resistance to the ring. When this happens some of them will also discharge to the metal ring. The figures show that this action lasts for 200-350 microseconds. Decay of the initial ionized path appears to be the limiting factor. If charge neutralization of the immediate area was the influencing factor, theory would permit the whole surface to be discharged. Figure 22 was taken of Teflon and bears out the path decay theory.

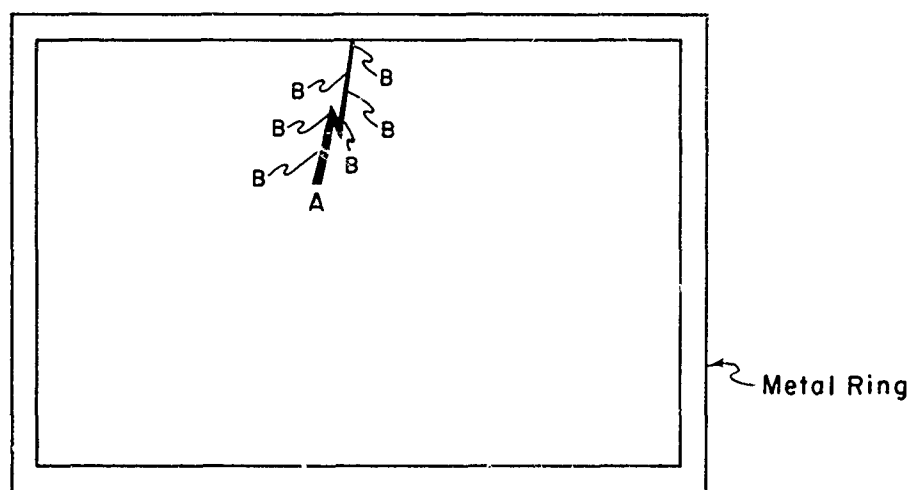


Figure 21. Illustration of Multiple Pulse Theory

By using the equations listed in Appendix III, we are now in a position to calculate the theoretical spectrum and compare it with that obtained experimentally. This is done in Figure 23. Appendix III contains a discussion concerning the differences between the theoretical and observed noise levels and possible causes.

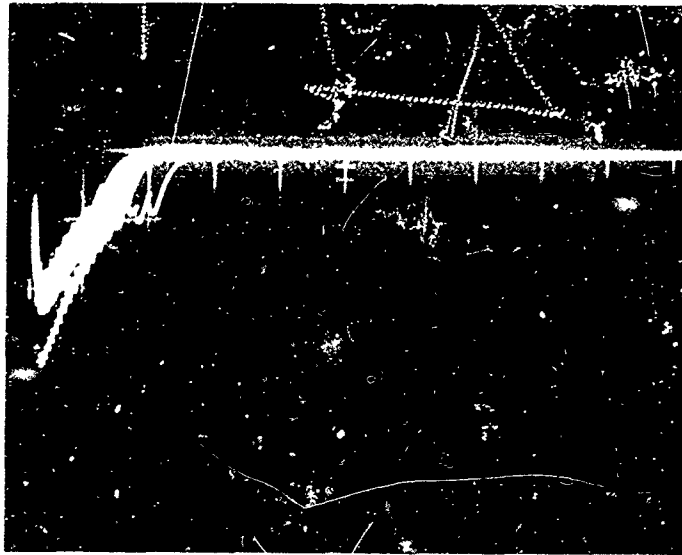


Figure 22. Teflon Pulse Path Decay

An interesting series of measurements was conducted on the charging currents. The current was measured through a 103,000-megohm resistor for equal area samples of copper, quartz, acrylic, alumina, epoxy, SMRFW(A), and the aircraft and missile nose cone samples. From the copper, we obtain a measure of the impact noise current. It should be essentially the same for all the samples. Any excess can be attributed to streamer noise. The results of this experiment are listed in Table X.

All samples showed electric field distributions after the air blast was stopped. Figure 24 shows the distribution obtained on a slab of quartz with the dielectric being larger than the standard size ring. The electrical tape was applied in three layers to the appropriate section of the sample on both sides in order to insulate it from the clamp assembly. For reference purposes, the ring is 2-1/2 inches by 5-3/4 inches. Figure 25 was taken of the epoxy sample. Here the field pattern is readily apparent.

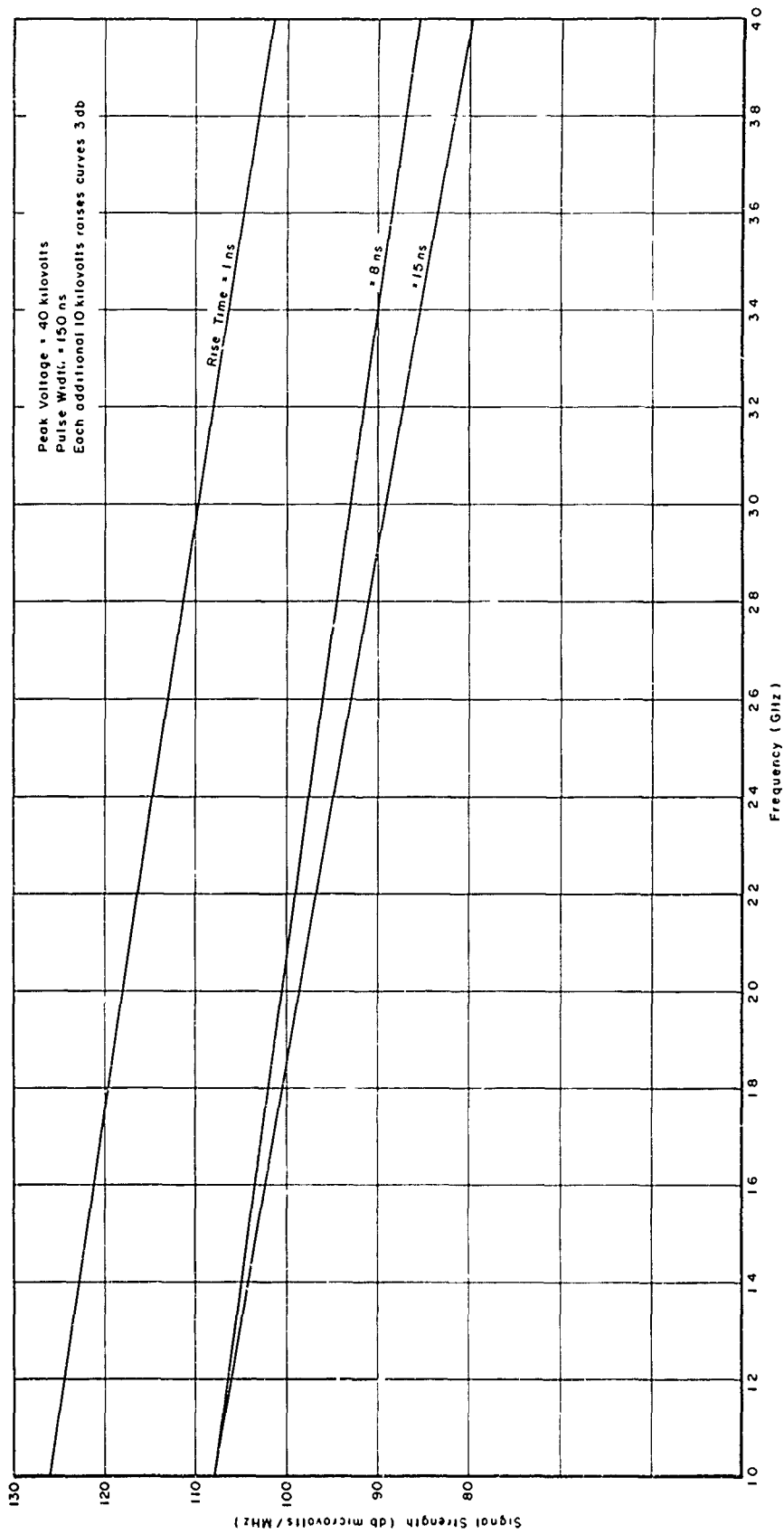


Figure 23. Theoretical Spectrum of Fast Rise-Time Pulses

TABLE X
DC CURRENTS OF SAMPLES

Material	Total Current (microamperes)	Computed Streamer Noise (microamperes)
Copper	.5 - .6	
Quartz	.8 - 1.2	.2 - .6
Acrylic	.9 - 1.4	.3 - .8
Alumina	.5	0
Epoxy	1.8 - 2.4	1.2 - 1.8
SMRFW (A)	1.4 - 2.0	.8 - 1.4
Aircraft sample	1 - 1.5	.4 - .9
Missile nose cone	.8 - .9	.2 - .3

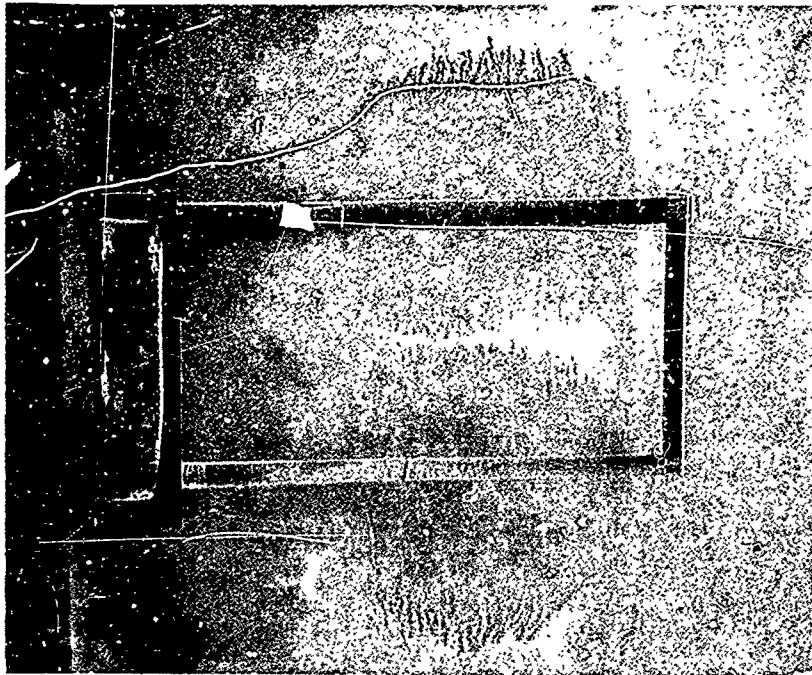


Figure 24. Quartz Static Field

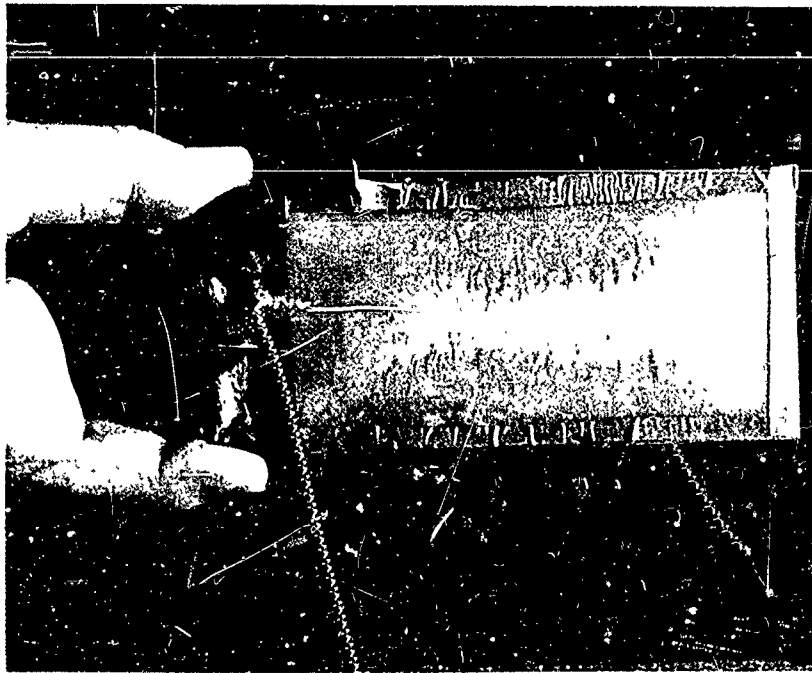


Figure 25. Epoxy Static Field

SECTION IX
TEST DIFFICULTIES TO BE EXPECTED

It is very doubtful that these test results could be repeated by another researcher. Such a statement is not intended to detract from their validity but is merely recognition of the many variables that exist some of which are now discussed.

Pulse amplitudes, rise times, shapes, duration, and repetition rates vary from material to material. These variables ultimately find their way into the final data curves even though techniques have been used to lessen their influence. The receiver would indicate the reception of a transient (hopefully single) pulse but closer examination would reveal the reception of 2-7 pulses which alone could account for reading variations of 10 db. No way was found to create a single streamer or to insure the reception of a single pulse. Threshold voltages are determined by the surface, charge pattern, air properties, and proximity to the collecting ring. The surface charge pattern in turn is determined by the surface resistivity, charging stream characteristics, and physical shape and dimensions. If the rise time and observed frequency are held constant and the peak pulse voltage is increased from 2 to 4 kilovolts, the effective broad-band equivalent signal level is changed by 6 db.

System losses vary due to the geometrical shape of the collecting ring and orientation of the streamering surface. The position of the air gun and external RF reflecting surface behind it may account for 1-2 db. Movement of the collector ring (sample positioning Method A) to coaxial adapter would affect the system losses 4-12 db. During the actual tests its movements were fairly well restricted and probably contributed 3 db variation.

Uniformity of the charging particles or stream could not be guaranteed. The flour was kept in an enclosed area free from large changes in ambient humidity and used until it became contaminated or showed a trace of agglutination. Microscopic examination revealed some expected physical changes. Prior to use, the average particle diameter was 5-8 mils (1025-1900 microns). After many cycles (10-20), the percentage of 5-mil particles was very small, the

predominate size being 1-2 mils or smaller. A reduction in particle size will result in increased particle concentration causing an increase in triboelectric charging RF noise.

A lesser problem is receiver gain stability. This factor was minimized by performing calibrations for each test.

The generation of reproducible microwave noise produced by triboelectric charging in the laboratory is no easy matter. During a portion of the tests, 28 MHz, 20 MHz, and 140 KHz were monitored in an effort to determine if the difficulty could be in the experimental configuration. Every blast of the air gun produced noise at each of these frequencies. No signal strength measurements were made at 20 and 28 MHz. Signal strengths at 140 KHz were approximately 150-170 db microvolts/MHz. The noise level at 1 GHz was monitored continuously. A coupling factor of -62 db was measured and the mean discernible sensitivity (MDS) of the receiver was -95 dbm, therefore, the minimum amount of noise generated on the surface that could be measured was the impulse noise equivalent of a -33 dbm CW signal or 74 db microvolt/MHz. Previous data for the same sample show generated noise levels of 87 db microvolt/MHz (pulse correction factor not accounted for). The pulse correction factor is approximately 25 db, i. e., the receiver reads 25 db low for single or very low repetition pulse trains.

The observed noise showed wide variations in signal strength. Figures 9 and 11 show the change in generated noise levels for quartz, epoxy, Teflon, and the aircraft sample for various tests. These curves are best fit lines and do not portray the complete picture. Figure 12 shows the generated signal strength envelope. A large range of values at a selected frequency is detected by even the casual observer.

One possible explanation for this difficulty could be the changing characteristics of the flour as it is cycled over and over. New flour was used with no observed change in noise levels. This variable can now be eliminated. Humidity (ambient) records were kept, 5-15%, and no discernible influence was detected.

The humidity of the compressed air stream was found to be that of the ambient humidity. The variables of particle velocity and concentration were essentially constant.

During the testing program, the 140 kilohertz noise level would drop 4-10 db for no apparent reason and remain at that level. At both levels (high and low), the received signal strengths varied 1-3 db and could be considered as being constant. The mechanism causing this drop in 140-KC noise was sufficient to eliminate microwave reception.

It was common for the five readings taken at each frequency at the same time to vary up to 7-14 db or to stay in the range of 1-3 db. Readings taken on successive days showed a 1-23 db variation at the same frequency.

Two other variables may have a part in this seemingly unexpected behavior. Space charges built up by cumulative ionization preceding the discharge will cause a lowering of the breakdown threshold. Sparks produce nitric oxides which can lower the threshold by 5% or more (Reference 15). This is due to the fact that the ionization potentials of N_2 and O_2 are in the neighborhood of 15.5 and 12.5 volts, respectively, whereas that of NO is 9.5 volts and other nitrogen oxides are still lower. The other possible variable may be that of uniform air purity. No extra steps were taken to assure that the above problems were not present. One would expect that the force of the air stream would clear the space around the sample of space charge and nitric oxides. This reasoning would not explain the complete absence of measurable microwave noise on certain days. The air purity was that of typical winter days; i.e., no observable visible smog.

The conclusions to be drawn from this discussion are that the physics of the simulated test are not sufficiently accurate to describe the actual environmental conditions; however, based upon information obtained from other sources, the simulation is a reasonable approximation for design considerations. Flight testing will be required if greater accuracy than what was obtained during these tests is required.

SECTION X
CONCLUSIONS AND RECOMMENDATIONS

1. CONCLUSIONS

The following conclusions are drawn as a result of this particular laboratory study.

a. Triboelectric noise (microwave) is subject to widespread variations. The derived signal strengths should be taken as a minimum. A suitable safety factor would be 10-20 db.

b. Coupling factors in a setup of this type should be taken every time a test is run.

c. Mounting the samples on a ground plane produces results superior to those obtained in free space.

d. The amount of dielectric surfaces should be kept to a minimum for another reason, electromagnetic pulse (EMP). EMP is produced by detonation of nuclear bombs and nearby lightning strokes. The metallic fuselage acts as a faraday cage resulting in the protection of internal equipments. Dielectrics, on the other hand, offer no such protection. Therefore, restraint must also be used in the amount of dielectric. In this case what might be a remedy for one problem may open up another serious problem.

e. Approximately 15 db improvement is offered by the coarse slotted metallic RF window (A) over Teflon. This study should not be considered as the ultimate test of this concept for the reduction of precipitation static at microwave frequencies. The noise generation is dependent on the dielectric base, size, and geometrical configuration of the slots and their density.

f. Epoxy formulations show a wide distribution of noise levels. Therefore, they should not be chosen indiscriminately.

2. RECOMMENDATIONS

The following suggestions for future work in this area are offered:

a. This work should be repeated and/or expanded in an isolated environment equivalent to that experienced by the aircraft, i.e., 0% humidity and 20°F or lower. Facilities at WPAFB may prove to be ideal.

b. Reception by a field strength receiver especially designed for the reception of impulsive noise should be used. Its use would have eliminated the time-consuming pulse counting and calibrating procedures.

c. Aircraft manufacturers appear to be convinced that the aircraft of the future will have more and more dielectric surfaces and less metallic surfaces. Such a vehicle could possibly be useless from the viewpoint of LORAN, ILS, HF and VHF communication performance, and lightning damage. There is a relatively simple possible solution to the problem. It consists of laminating a thin sheet of metal to the surfaces that are not required to be transparent to RF. If this was done with the equivalent of 1 oz of aluminum/ft² (a typical printed circuit board contains 1 oz of copper/ft²), the weight penalty would be about 6.25 lbs/100 ft². The specific gravity of aluminum is 33% that of copper. If the metallic surface such as found on a printed circuit board was deemed to be sufficient, the weight penalty could be cut to slightly more than 2 lbs/100 ft². This surface treatment will cost money; so do aircraft (original purchase or replacement), retrofits, modifications, grounded aircraft, and lawsuits based on inadequate commercial aircraft and mistakes. Numerous examples can be cited in each category.

d. For RF transparent surfaces, the slotted metallic RF window concept offers a great deal of promise. The anticipated lower frequency limit is S band. This device possesses many other desirable features that will not be cited because they are not germane to the problem.

e. Optical windows, especially quartz, are a serious problem if remedial steps are not taken. One proven method is the coating of the outside surface with

a thin film of stannous oxide or other suitable optically transparent, low surface resistivity material. Streamer pulses also generate light. On some systems the generation of light may be more of a problem than that of RF noise generation.

f. The materials people should develop conductive epoxies with resistivities equal to that of antistatic coatings in present use. Conductive epoxies are not unrealistic and they do exist; however, the work to date has consisted primarily of attempting to develop epoxies with conductivities approaching that of good conductors (Reference 16).

g. Wind tunnel studies should be used to find positions on the airframe that are not subject to triboelectric charging in flight. Dielectric surfaces may be placed at these points and will produce a minimum of interference. This method may be too expensive to be performed on troublesome vehicles. In many cases, the locations of dielectric surfaces are fixed by operational considerations. Such a method of attack would find its greatest usefulness in the preliminary and early design stages.

h. If the position of dielectric surfaces is fixed, coupling factor measurements should be made on a scale model to determine the expected level of interference produced in other on-board systems and/or to find the best placement for other antennas. Again desired operational characteristics may be the overriding factor.

i. A widespread (civilian and military) reporting system should be established in an effort to determine the full operational impact of triboelectric interference. Items of interest are weather conditions, type of aircraft, frequency of interference, type of interference, altitude, velocity, etc. This technique may be able to correctly classify the trouble (p-static--yes or no) at an early stage of the investigation, produce documented evidence of its scope and magnitude, and provide a possible method of attack in reducing p-static problems on future aerospace vehicles.

j. Operating personnel should be encouraged to report instances in which observed interference may be due to triboelectric charging.

k. The phenomenon of triboelectric charging and its consequences needs to be widely disseminated particularly among personnel involved in the designing of future aircraft, installing RF equipment aboard the vehicle, and modifying existing vehicles. This may be done by technical reports, memoranda, or meetings. Part of the present difficulty may be due to the familiarity of p-static and triboelectric charging being limited to a relatively small number of people. Anyone having a possible part in its production should have at least heard of the phenomenon and be aware of its consequences.

APPENDIX I

DISCUSSION OF SPARKING MECHANISM

The term surface breakdown means the development of a conducting channel between two electrodes on a dielectric surface. In this study these electrodes are two points of different potential or one point of voltage potential and the local ground. Surface breakdown may be divided into flashover and tracking. Flashover involves essentially a gaseous discharge but does not necessarily impair permanently the insulating properties of the surface. Tracking requires that the conducting channel lie wholly or mainly in the dielectric surface which suffers damage in the process.

Flashover is a gaseous discharge with more or less interaction between it and the solid dielectric. When the electric field has a high enough value near the dielectric surface, the discharge clings to the surface.

There are two types of tracking: high voltage and low voltage. The latter may involve no discharge at all since it can take place at voltages less than the minimum breakdown voltage of the medium. It arises from the presence of conducting paths. In high voltage tracking, the conducting path is begun by the impinging of a discharge on the dielectric surface. Since organic dielectrics are the more subject to tracking than inorganic dielectrics, carbonized conducting paths are those most frequently met.

There is a good deal of evidence that discharges in a gas bounded by insulating material occur at potentials of order similar to those required with metal electrodes and, provided there is adequate charge available on the dielectric surfaces, have much the same properties in the transitory regime as discharges between metal electrodes. Therefore, a spark discharge should neutralize the surface charges near the ends of the discharge. High surface resistivity may limit the area discharged, and surrounding areas will tend subsequently to restore the potential. Some experiments have shown that the potential gradient remaining after discharge to be 500 volts/cm to several kilovolts/cm. Dawes and Humphries (Reference 17), who exposed large areas of dielectric to discharges, say that the remanent potential is some 50-80% of the potential required

to start the discharge. This behavior was observed during the testing program. Its main effect is to cause initiation of subsequent discharges to be easier than the first because they are taking place on a biased surface. The remaining potential was from 0-35% of that necessary to start the discharge.

In a fairly uniform field, a discharge usually develops into a spark if enough energy is available. A generally accepted equation for spark breakdown in a plane parallel gap at atmospheric pressure is

$$X_s \left(\frac{\delta}{p} \right)^{\frac{1}{2}} = 5.27 \times 10^{-7} \frac{a}{p} e^{\frac{a\delta}{p}}$$

where X_s = sparking field (volts/cm)

δ = gap length (cm)

p = pressure (mm of Hg)

a = constant dependent on the subject gas (about 18.6 for air)

so that

$$a + \ln \frac{a}{p} = 14.46 + \ln X + \frac{1}{2} \ln \frac{\delta}{p}$$

where X = field strength for breakdown

For any other field distribution, streamer formation will follow when the electron avalanche has traversed a length d such that

$$X_s = 5.27 \times 10^{-7} \frac{a_d e^{\int_0^d a dx}}{\sqrt{\frac{d}{p}}} \text{ volts/cm}$$

where a_d = value of a at the end of the avalanche.

The investigation of the conditions for the generation of negative corona may give some clue as to the reason for the difficulties encountered in this program. Negative corona will be produced when the following conditions are met

$$a dx + \ln a_0 = 12.16 + \ln \frac{X_0}{p} + \frac{1}{2} \ln pa$$

where X_0 and a_0 are the value of X and a at the point distance a centimeters from the surface of the electrode. For air at 760 mm Hg, this expression reduces to

$$a dx = 18.9 + \frac{1}{2} \ln (pa)$$

In this investigation the atmospheric pressure change was so small that it could be considered to be a constant (refer to the above equations). The only other variable that could possibly account for the difficulty is a . The variable a is a measure of the electron avalanche characteristics of the gas under certain specified conditions and depends on pressure, the gas, photoionization, distance from electrodes, and field strength. The first four factors can be discounted. Field strength variation appears to be the culprit. Peak pulse values of 30-100 kilovolts have been observed. Examination of Table XI will show the rapid variation of a with X/p . Thus we have proven something which was intuitively suspected.

TABLE XI
VARIATION OF a WITH X/p

X/p (volts/cm per mm Hg)	a
26	.2
28	.4
30	.7
32	1.6
34	2.5
36	6.2
40	13
45	25
50	38
55	64

Air at 760 mm Hg and 22°C

APPENDIX II

NATURAL VERSUS ARTIFICIAL ENVIRONMENT

The basis for the naturally occurring environment is found in past reports issued by Stanford Research Institute (SRI) and are listed in the references.

Particle concentrations are listed as 2×10^4 particles/m³ for the typical cirrus cloud and $6-12 \times 10^4$ particles/m³ for a thunderhead (Reference 20). A check of many current texts on meteorology revealed no data on particle concentrations. The estimated density factor for a 1 megaton nuclear surface blast is 3×10^{-8} grams/cc immediately after detonation to 3×10^{-9} grams/cc 24 hours detonation (Reference 1, Part I).

The experimentally derived particle density is shown in Figure 26. The observed skewness of the density profile is due to the 45° mounting angle of the sample with respect to the charging stream; therefore, the particle impingement velocity is not constant giving rise to a change in particle concentration. A difference factor of 100 appears between the SRI reported particle density and that measured in the laboratory test setup.

The computed difference between the model and the nuclear cloud is of the same order of magnitude.

Recent atmospheric and meteorological research depicts a portion of the natural environment encountered in triboelectric charging of aircraft surfaces as follows. Average charge values for continuous rain are of the order of 10^{-16} coulombs/m³ while in showers and storms the averages reach nearly 10^{-15} coul/m³. The ratio of positive to negative charges varies from 1.3 to 1.8. Additional characteristics of precipitation are listed in Table XII. No data was found on electrical characteristics of airborne dust particles, fog, or ice crystals.

The other primary charging mechanism, particularly around storm centers, is the high electric fields associated with such disturbances. Such field intensities

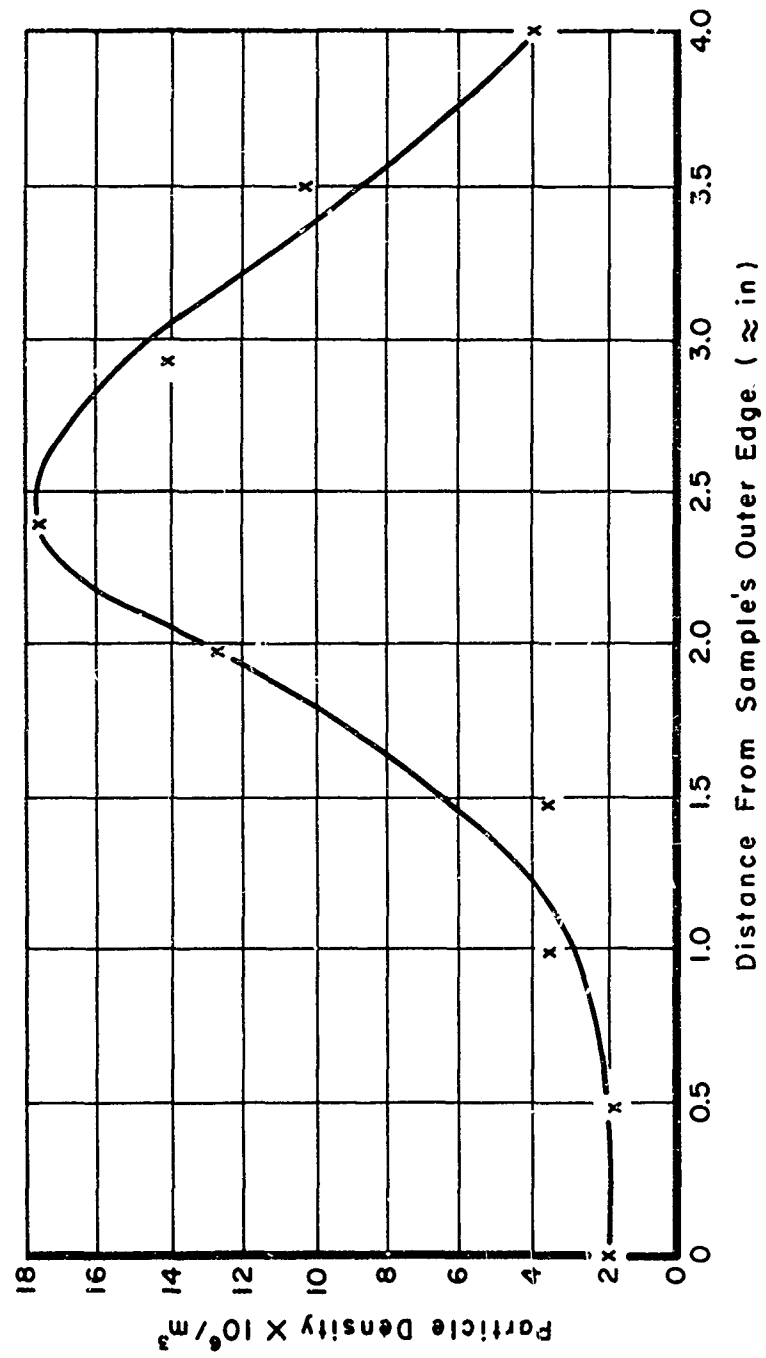


Figure 26. Particle Density Profile

TABLE II

AVERAGE FREE ELECTRICAL CHARGE ON INDIVIDUAL DROPLETS

Altitude (ft)	Charge	Quiet Rain*	Shower Rain*	Electrical Storm Rain*	Quiet Snow Fall*	Squall Snow Fall*
Surface	+	0.6 - 6.6	4.2 - 19	12 - 50	0.3 - 1.7	16 - 30
	-	1.5 - 10	7.5 - 21	19 - 60	0.2 - 3.3	15 - 19
4000	+					
	-		80			
5000	+			267		
	-			208		
10,000	+			488		
	-			370		
12,000	+		136			
	-		330			
15,000	+			406		
	-			250		
20,000	+		208	172		
	-			208		

*All values 10^{-13} coulombs

have been measured up to 6000 volts/m. These fields may produce a bias on the dielectric surface which in turn will reduce the particle concentration and/or velocity needed to produce precipitation static interference.

All of the tests reported were conducted at approximately 1000 ft elevation. The dependence of temperature and air pressure with altitude is well known. The principal variables that determine whether a sparking condition exists are examined in Appendix I. Ambient pressure plays a very important role. Table XIII lists the variation of breakdown voltage with air pressure (altitude). Temperature is also expected to be important because it should affect the relative humidity and possibly the ion mobility.

TABLE XIII

BREAKDOWN VOLTAGE VERSUS ALTITUDE

Air Pressure (mm Hg)	Breakdown Voltage (volts/cm)
760	32,200
380 = 5,500 ft	18,600
200 = 9,900 ft	11,100
100 = 14,300 ft	6,550

This little exercise is not intended to uphold nor destroy the validity of the work being reported. It was conducted out of curiosity. The important fact to be remembered is that this test configuration yielded charging currents and pulse repetition rates that could be correlated with those values actually obtained in flight at approximately equal particle velocities.

Future efforts designed to find a higher charging medium may be useful in an attempt to actually measure noise levels at higher frequencies.

APPENDIX III

DERIVATION OF THEORETICAL SPECTRUM

The following discussion on development of the theoretical RF spectrum was derived by Luis Oh (Reference 14) under sponsorship of the Air Force Avionics Laboratory. It is not reproduced in complete form but the essential points required for the spectrum calculations are listed.

A general expression for the discharge voltage is:

$$V(t) = V_p \left[\frac{t}{t_1} \{ u(t) - u(t-t_1) \} + e^{-\alpha(t-t_1)} u(t-t_1) \right]$$

where V_p = peak pulse voltage.

The Fourier transform of $V(t)$ is:

$$V(\omega) = V_p \left[\int_0^{t_1} \frac{t}{t_1} e^{-j\omega t} dt + \int_{t_1}^{\infty} e^{-\alpha(t-t_1)} e^{-j\omega t} dt \right]$$

$$V_p \left\{ \frac{1}{t_1 \omega^2} \left[e^{-j\omega t_1} (j\omega t_1 + 1) - 1 \right] + \frac{1}{\alpha + j\omega} e^{-j\omega t_1} \right\}$$

We are only interested in positive frequencies; therefore, the following restriction must be used,

$$|V(\omega)| = 2V_p \left\{ \left[\frac{1}{t_1 \omega^2} (1 - \cos \omega t_1) + \frac{\alpha}{\alpha^2 + \omega^2} \right] + \left[\frac{1}{t_1 \omega^2} (\omega t_1 - \sin \omega t_1 - \frac{\omega}{\alpha^2 + \omega^2}) \right]^2 \right\}^{\frac{1}{2}}$$

For the high frequency range ($f \gg 10^8$ Hz), this expression can be reduced as shown below.

$$\omega t_1 \gg \sin \omega t_1$$

Choose w to make $\cos wt_1 = 0$ and $\sin wt_1 = 1$

$$\begin{aligned} |V(w)| &= 2V_p \left[\left(\frac{1}{t_1 w^2} + \frac{\alpha}{\alpha^2 + w^2} \right)^2 + \left(\frac{1}{w} - \frac{w}{\alpha^2 + w^2} \right)^2 \right]^{\frac{1}{2}} \\ &= 2V_p \left[\frac{\alpha^2 + (1 + t_1 \alpha)^2 w^2}{t_1^2 w^4 (\alpha^2 + w^2)} \right]^{\frac{1}{2}} \\ &\approx 2V_p \frac{1 + t_1 \alpha}{t_1 w^2} \end{aligned}$$

From Table IX we see that t_1 (pulse rise times) varies from 4 to 16 ns (actually 1.7 to 17 ns - Table III). Alpha is the reciprocal of pulse time constant (approximately 50 - 80 ns).

Sample calculation: Epoxy

$$t_r = 8 \text{ ns} \quad \text{pulse width} = 150 \text{ ns} \quad w = 6.28 \times 10^9 = 1 \text{ GHz}$$

Peak voltage = 40 kilovolt (obtained by voltage division between the 50-ohm load and oscilloscope)

$$\begin{aligned} |V(w)| &\approx 8 \times 10^4 \frac{1 + 8 \times 10^{-9} \left(\frac{1}{75 \times 10^{-9}} \right)}{8 \times 10^{-9} (3.95 \times 10^{19})} \\ &= \frac{8.8 \times 10^4}{3.16 \times 10^{11}} = 28 \times 10^{-8} \text{ V/Hz} \\ &= 28 \times 10^{-2} \text{ V/MHz} \\ &= 109 \text{ db } \mu\text{V/MHz} \end{aligned}$$

This value is 8 db lower than the computed signal strength in Figure 11. The data in Figure 11 was derived from an average value of the receiver's pulse response, and the receiver indicated signal strength (received) is integrated over multiple pulses (1-5). Only one selected pulse was used in the above calculation.

A look at the list of variables that could possibly account for this 8-db variation will show that no precise agreement between the theoretical and measured signal strengths is expected. The list of variables is given below.

1. Peak pulse voltage
 2. Pulse rise time
 3. Number of pulse/discharge (actual)
 4. Receiver pulse calibration (average value taken over all samples)
 5. All pulses may have significantly different parameters
 6. Method of measuring pulse rise times may have influenced the results
 7. A combination of the above
- } selected pulse

In Figure 11 the total signal level change from 1 - 4 GHz varies from 17 - 22 db, with one exception. This is in good agreement with the theoretical value of 24 db. In all cases the extreme randomness of the process should be remembered.

REFERENCES

1. J. E. Nanevicz, E. F. Vance, W. C. Wadsworth, and J. A. Martin. Low Altitude Long Range All-Weather Vehicle Interference Investigation. SRI Project 5082. Prepared by Stanford Research Institute. AFAL-TR-65-239, Part I (December 1965) and Part II (December 1966). AF Avionics Laboratory, Wright-Patterson AFB, Ohio.
2. Ye. V. Chubarina and I. M. Imyanitov. Electricity of the Free Atmosphere (Results of Measurements During the IGY and MGC). English Translation of Russian Text. FTD-MT-24-156-68. Foreign Technology Division. Wright-Patterson AFB, Ohio. 21 August 1968.
3. J. D. Craggs and J. M. Meek. High Voltage Laboratory Technique. Butterworths Scientific Publications, London. 1954.
4. CH-54 (Flying Crane) Electrostatic Discharger Evaluation. ECOM-3120. April 1969.
5. J. E. Nanevicz and R. L. Tanner. Radio Noise Generated on Aircraft Surfaces. SRI Project 1267. Final Report on Contract AF 33(616)-2761, prepared by Stanford Research Institute, Menlo Park, California. September 1956.
6. Kent Rogers. Slotted Metallic RF Window Investigation. AFAL-TR-70-13. Prepared by Texas Instruments Inc. on Contract F33615-69-C-1591. AF Avionics Laboratory, Wright-Patterson AFB, Ohio. To be published.
7. "Insulating Materials." Electronic Design, Vol 17, No. 12. Hayden Publishing Company, New York. 7 June 1969.
8. Charles A. Harper. Plastics for Engineers. Kiner Publications Inc., Chicago, Illinois. 1964.
9. Charles A. Harper. Electronic Packaging With Resins. McGraw-Hill Book Company, Inc., New York. 1961.
10. Plastics Reference Issue. Machine Design. 12 December 1968.
11. Reference Data for Radio Engineers. 5th Edition. Howard W. Sams and Company Inc., New York. 1968.
12. Charles A. Harper. "Electrical Insulating Materials." Machine Design. 28 September 1967.
13. CRC Handbook of Chemistry and Physics. 46th Edition. Chemical Rubber Company, Cleveland, Ohio. 1965.

REFERENCES (CONTD)

14. Reuben Goldman, George C. Huang, Luis Oh, et al. Natural and Induced Electrical Effects on Integrated Antennas and Circuits at Frequencies to 10 GHz. AFAL-TR-69-210. Prepared by The Boeing Company on Contract F33615-68-C-1720. AF Avionics Laboratory, Wright-Patterson AFB, Ohio. September 1969.
15. Leonard B. Loeb and John M. Meek. The Mechanism of the Electric Spark. Stanford University Press, Stanford University, Stanford, California. 1941.
16. "Conductive Plastics." Machine Design. 16 October 1969.
17. S. Whitehead. Dielectric Breakdown of Solids. Oxford University Press, London. 1951.
18. Thomas F. Malone et al. Compendium of Meteorology. American Meteorological Society, Boston, Mass. 1951.
19. J. Alan Chalmers. Atmospheric Electricity. Pergamon Press. 1957.
20. J. E. Nanevicz and R. L. Tanner. Precipitation Charging and Corona-Generated Interference in Aircraft. AFCRL 336 Technical Report 73. SRI Project 2594. Prepared by Stanford Research Institute on Contract AF 19(604)-3458. AF Cambridge Research Laboratories. April 1961.
21. Samuel C. Coroniti, James Hughes, et al. Planetary Electrodynamics. Gordon and Breach Science Publishers, New York. 1969.
22. J. E. Nanevicz. A Study of Precipitation-Static Noise Generation in Aircraft Canopy Antennas. AFCRC-TN-56-583, AD 133 623. Technical Report 62, SRI Project 1197. Prepared by Stanford Research Institute on Contract AF 19(604)-1296. Cambridge Research Center. December 1957.
23. Lightning and Static Electricity Conference, 3-5 December 1968. Part II, Conference Papers, AFAL-TR-68-290. AF Avionics Laboratory, Wright-Patterson AFB, Ohio. May 1969.
24. Mischa Schwartz. Information Transmission, Modulation, and Noise. McGraw-Hill Book Company, Inc., New York. 1959.
25. M. P. Amason. Douglas Aircraft Company Lightning Protection Research and Development Capabilities. Douglas Paper 5692, Douglas Advanced Research Laboratories, McDonnell Douglas Corporation, Huntington Beach, California. November 1969.
26. Charles P. Smyth. Dielectric Behavior and Structure. McGraw-Hill Book Company, Inc., New York. 1955.
27. Minzner, Champion, and Pond. The ARDC Model Atmosphere, 1959. AFCRC-TR-59-267. AF Cambridge Research Center, Bedford, Mass. August 1959.

UNCLASSIFIED

Security Classification

DOCUMENT CONTROL DATA - R & D		
<i>(Security classification of title, body of abstract and indexing annotation must be entered when the overall report is classified)</i>		
1. ORIGINATING ACTIVITY (Corporate author) Air Force Avionics Laboratory (AFAL/WRE) Wright-Patterson AFB, Ohio 45433		2a. REPORT SECURITY CLASSIFICATION Unclassified
		2b. GROUP
3. REPORT TITLE TRIBOELECTRIC CHARGING OF AIRCRAFT DIELECTRIC SURFACES IN THE MICROWAVE FREQUENCY REGION (1-4 GHz)		
4. DESCRIPTIVE NOTES (Type of report and inclusive dates)		
5. AUTHOR(S) (First name, middle initial, last name) Larry E. Cummings		
6. REPORT DATE October 1970	7a. TOTAL NO. OF PAGES 71	7b. NO. OF REFS 28
8a. CONTRACT OR GRANT NO.	9a. ORIGINATOR'S REPORT NUMBER(S) AFAL-TR-70-137	
b. PROJECT NO. 4357		
c. Task No. 435706	9b. OTHER REPORT NO(S) (Any other numbers that may be assigned this report)	
d.		
10. DISTRIBUTION STATEMENT This report is subject to special export controls and each transmittal to foreign governments or foreign nationals may be made only with prior approval of the Air Force Avionics Laboratory (AFAL/WRE), Wright-Patterson AFB, Ohio 45433.		
11. SUPPLEMENTARY NOTES	12. SPONSORING MILITARY ACTIVITY Air Force Avionics Laboratory Wright-Patterson AFB, Ohio 45433	
13. ABSTRACT <p>Triboelectric charging can cause serious problems to modern aircraft. This work effort attempts to determine the RF spectral content of streamers produced on various dielectric materials that are being used or could be used on future high performance aircraft. These values are found to be in good agreement with the theoretically derived spectrum.</p> <p>This investigation covered the frequency range of 1.0 GHz to 4.0 GHz. Such a range is convenient in that it starts where other researchers have stopped and gives a good indication of expected signal levels at higher frequencies. A more detailed study could also be conducted due to the small frequency span.</p> <p>The first part of this report discusses the experimental setup and the rationale for the procedures used. Based on the experimental values obtained, definite recommendations are made for the reduction of precipitation static interference. The values obtained show a close correlation with flight test data.</p>		

DD FORM 1473

FORM
1 NOV 65

UNCLASSIFIED

Security Classification

14 KEY WORDS	LINK A		LINK B		LINK C	
	ROLE	WT	ROLE	WT	ROLE	WT
Precipitation Static Triboelectric Charging Streamering Naturally Produced Microwave Noise Dielectrics						